

Quantum thermal transport in nanostructures

Jian-Sheng Wang^{1,a}, Jian Wang², and J. T. Lü¹

¹ Center for Computational Science and Engineering and Department of Physics, National University of Singapore, Singapore 117542, Republic of Singapore

² College of Physical Science and Technology, Yangzhou University, Yangzhou 225002, P. R. China

Received: 20 February 2008 / Revised version: ??

Abstract. In this colloquia review we discuss methods for thermal transport calculations for nanojunctions connected to two semi-infinite leads served as heat-baths. Our emphases are on fundamental quantum theory and atomistic models. We begin with an introduction of the Landauer formula for ballistic quantum transport and give its derivation from scattering wave point of view. Several methods (scattering boundary condition, mode-matching, Piccard and Caroli formulas) of calculating the phonon transmission coefficients are given. The nonequilibrium Green's function (NEGF) method is reviewed and the Caroli formula is derived. We also give iterative methods and an algorithm based on a generalized eigenvalue problem for the calculation of surface Green's functions, which are starting point for an NEGF calculation. A systematic exposition for the NEGF method is presented, starting with the fundamental definitions of the Green's functions, and ending with equations of motion for the contour ordered Green's functions and Feynman diagrammatic expansion. In the later part, we discuss the treatments of nonlinear effects in heat conduction, including a phenomenological expression for the transmission, NEGF for phonon-phonon interactions, molecular dynamics (generalized Langevin) with quantum heat-baths, and electron-phonon interactions. Some new results are also shown. We also briefly review the experimental status of the thermal transport measurements in nanostructures.

PACS. 05.60.Gg quantum transport – 44.10.+i heat conduction – 65.80.+n thermal properties of small particles, nanocrystals, and nanotubes

1 Introduction

The first quantitative description of the phenomenon of heat conduction was given by Fourier in the early 1800s, which states that the heat current is proportional to the temperature gradient, $J = -\kappa \nabla T$. The coefficient, κ , is known as the thermal conductivity. Together with energy conservation, the temperature field of a macroscopic body satisfies a diffusion equation. Debye proposed simple kinetic theory to express the thermal conductivity in terms of a product of specific heat, velocity, and mean free path of the phonons. A more complete theory is given by Peierls [1], based on a Boltzmann equation for the phonons. The Boltzmann-Peierls equation approach for understanding the thermal transport has been a standard approach, and has been perfected by many people [2]. There is also recent work for a more rigorous derivation of the Boltzmann equations [3].

In recent years, much research has been done on mesoscopic to microscopic systems, including thermal transport [4,5,6], for the obvious reason of relevance to the

miniaturization in the electronic industry. At small scale, some of the concepts familiar at macroscopic regime may not be applicable, e.g., the concept of a distribution function of both coordinate and momentum used in the Boltzmann equation. At the nanoscale, where atomic detail becomes important, we expect to replace the Boltzmann equation by something more fundamental. One possibility is quantum Boltzmann equations [7,8]. Another class of methods for thermal transport problems starting with atomic models is molecular dynamics (MD) [9,10,11]. The thermal conductivity can be computed in equilibrium based on the Green-Kubo formula, or through a direct computation of the thermal current in a nonequilibrium setting. A variety of systems has been simulated with MD for nanostructures and interfaces. However, since MD is purely a classical method, quantum effect can not be taken into account.

In this review, we consider a bottom-up approach where we start with a lattice model with only the harmonic interactions. Such models explain well the thermal transport properties when systems under consideration are smaller than their mean free path of the phonons. This regime is known as ballistic heat transport regime. This will be the contents of Sec. 2. In this section, we discuss the con-

^a also at Institute of High Performance Computing, 1 Science Park Road, Singapore 117528, and Singapore-MIT Alliance, 4 Engineering Drive 3, Singapore 117576.

cept of universal thermal conductance for perfect ballistic systems, and address the issue of computing the thermal current if the system is not a perfect periodic lattice. The result is given by the Landauer formula. Effective computational methods will be reviewed for the transmission coefficient used in the Landauer formula. What will happen if we introduce interactions for the phonons? We discuss this issue in Sec. 3. The problem of nonlinear interaction can be solved, at least in principle, with the nonequilibrium Green's function (NEGF) method, which is more fundamental than the Peierls approach, and without conceptual difficulty. In practice, the NEGF method is computationally extremely intensive if the nonlinear problem is treated by mean field approximations. We also review a new molecular dynamics method where quantum effect can be taken into account approximately. In particular, the ballistic regime can be simulated correctly. Electron-phonon interaction, as well as recent experimental progress, will be reviewed briefly.

1.1 Models in this review

For notational consistency, in this review, we'll discuss a model of junction connected to two leads using the following Hamiltonian [12,13]. The model is in fact very general. In order to have a form for the Green's function similar to that of electrons, we use a transformation for the coordinates, $u_j = \sqrt{m_j} x_j$, where x_j is the relative displacement of j -th degree of freedom having the dimension of length, and we call u_j the mass-normalized displacement. In this way, the kinetic energy is always of the form $\frac{1}{2}\dot{u}^T \dot{u}$ (where the superscript T stands for matrix transpose), and the mass information is transferred completely to the spring constants. We introduce a superscript α to indicate the region. Then u_j^α is the deviation from equilibrium position for the j -th degree of freedom in the region α ; $\alpha = L, C, R$, for the left, center, and right regions, respectively. The quantum or classical Hamiltonian is given by

$$\mathcal{H} = \sum_{\alpha=L,C,R} H_\alpha + (u^L)^T V^{LC} u^C + (u^C)^T V^{CR} u^R + V_n, \quad (1)$$

where $H_\alpha = \frac{1}{2}(\dot{u}^\alpha)^T \dot{u}^\alpha + \frac{1}{2}(u^\alpha)^T K^\alpha u^\alpha$ represents coupled harmonic oscillators, u^α is a column vector consisting of all the displacement variables in region α , and \dot{u}^α is the corresponding conjugate momentum. K^α is the spring constant matrix and $V^{LC} = (V^{CL})^T$ is the coupling matrix of the left lead to the central region; similarly for V^{CR} . The dynamic matrix of the full linear system is

$$K = \begin{pmatrix} K^L & V^{LC} & 0 \\ V^{CL} & K^C & V^{CR} \\ 0 & V^{RC} & K^R \end{pmatrix}. \quad (2)$$

There will be no interaction between the two leads. The nonlinear part of the interaction will take the form

$$V_n = \frac{1}{3} \sum_{ijk} T_{ijk} u_i^C u_j^C u_k^C + \frac{1}{4} \sum_{ijkl} T_{ijkl} u_i^C u_j^C u_k^C u_l^C \quad (3)$$

for perturbation expansion, but it can be arbitrary. Notice that the notation is valid independent of the actual physical dimensions used.

For easy treatment, we consider the leads as quasi-one-dimensional lattices characterized by three square matrices of equal size, k_{00} , k_{11} , and k_{01} . The matrix k_{00} is the block immediately adjacent to the center, while k_{11} , and $k_{01} = k_{10}^T$ are repeated for the semi-infinite chain of the lead. They form the whole dynamic matrix of the lead in the following way:

$$K^R = \begin{pmatrix} k_{00} & k_{01} & 0 & \cdots \\ k_{10} & k_{11} & k_{01} & 0 \\ 0 & k_{10} & k_{11} & k_{01} \\ \cdots & 0 & k_{10} & \ddots \end{pmatrix}. \quad (4)$$

If there are some irregularities in the junction structure, we can enlarge the central part, so that the lead is always a regular lattice. The nearest neighbor nature of K^R is not a real limitation, since one can use a large supercell so that only the neighbor cells have interactions. If the cross sections of the leads are large, we can also model bulk walls.

The semi-infinite nature of the leads is important conceptually. First, the heat bath by definition must be sufficiently large so that any finite energy transfer does not affect its temperature. Second, phonon waves scattered back into the bath will get dissipated and will not be reflected back to the central region. Any finite harmonic system will not have such a property.

2 Ballistic thermal transport

2.1 Landauer formula

As early as 1957, Rolf Landauer presented a very intuitive interpretation of electron conduction in nanoscale junctions based on the concept of wave scattering [14,15]. The same argument can be applied to the phonon transport as well [16,17,18,19,20]. Heat current flowing from left to right through a junction connected to two leads at different equilibrium heat-bath temperatures T_L and T_R is given by the Landauer formula

$$I = \int_0^\infty \frac{d\omega}{2\pi} \hbar\omega T[\omega] (f_L - f_R), \quad (5)$$

where $f_{L,R} = \{\exp[\hbar\omega/(k_B T_{L,R})] - 1\}^{-1}$ is the Bose-Einstein (or Planck) distribution for phonons, and $T[\omega]$ is known as the transmission coefficient (or transmittance). The formula describes the situation that the central region is small in comparison with the coherent length of the waves so that it is treated as purely elastic scattering without energy loss. The dissipation resides in the heat baths. We refer to such a situation as ballistic thermal transport. Note that the transmission coefficient is independent of the temperature. All the temperature dependences are in the distribution functions f_L and f_R .

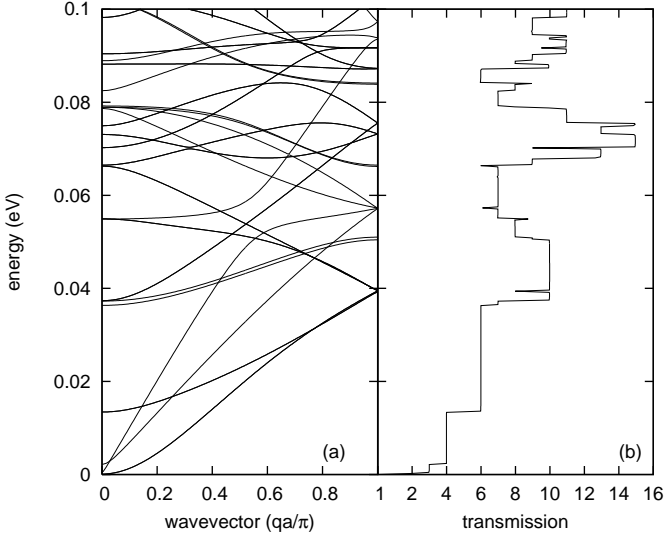


Fig. 1. (a) Dispersion relation $\hbar\omega$ vs. normalized wave number of a (6,0) carbon nanotube. (b) The phonon energy $\hbar\omega$ vs. the transmission coefficient $T[\omega]$.

The thermal conductance is defined as the limit

$$\sigma = \lim_{T_L \rightarrow T, T_R \rightarrow T} \frac{I}{T_L - T_R}. \quad (6)$$

The connection with the usual definition of thermal conductivity in the Fourier's law, $J = -\kappa \nabla T$, is, $\kappa = \sigma L/S$, where L is the length of a system in the direction of heat flow, while S is the cross-section area of the system. For quasi-one-dimensional systems like carbon nanotubes, σ is a better quantity to use, since the cross-section area S is not very well defined.

One very good use of the Landauer formula is that it provides an upper bound for the thermal conductance of quasi-one-dimensional periodic systems [21]. This is obtained when all modes of waves are transmitted without scattering or reflecting back to the heat bath. In this ideal situation, the transmission coefficient consists of a set of steps as a function of ω taking only integer values, that is

$$T[\omega] = \text{number of modes at frequency } \omega. \quad (7)$$

Figure 1(a) shows the dispersion relation of a carbon nanotube of chirality (6,0) with the force constants computed from Gaussian 03 [22]. We optimize a 7-period, hydrogen terminated structure. The basis set is 6-31G, and the theoretical model is b3lyp DFT method. Once the dispersion relation is computed, the transmission coefficient can be obtained by counting the numbers of positive wavevector branches of phonon vibrations. Actually, the transmission curve in Fig. 1(b) is calculated by a more general NEGF method, which will be discussed in Sec. 3.2.

In the low-temperature limit, the high energy optical modes will not be occupied due to the Bose-Einstein distribution. Only the lowest energy, long wave modes are important. In this low-temperature limit, we have $T[\omega] \approx N_m = 4$ for any quasi-one-dimensional systems possessing translational invariance in three directions and rota-

tional invariance along the axial direction (the four acoustic modes correspond to one longitudinal mode, two transverse modes, and an extra 'twist mode'), and the thermal conductance is given by

$$\sigma = \int_0^\infty \frac{d\omega}{2\pi} \hbar\omega N_m \frac{\partial f}{\partial T} = N_m \frac{\pi^2 k_B^2 T}{3h}, \quad (8)$$

independent of the material parameters. This is known as the universal quantum thermal conductance [17], in analogous to the universal electron conductance $2e^2/h$. The material constant independence stems from the fact that in one dimension, the product of phonon density of states and the group velocity is one. In higher dimensions, we must integrate in the k -space, instead of just a single ω [23]. The group velocity enters explicitly. The universality appears to have a deep connection to the maximum information or entropy flow in a channel [24,25]. The approximation $T[\omega] \approx 4$ is accurate when $k_B T$ is much smaller than the lowest optical mode energy $\hbar\Delta\omega$. For typical carbon nanotubes, this is valid when temperature is of order of few kelvin to 10 K. For Si nanowires with transverse dimension of few hundreds nanometers, it is below 1 K. The spacing $\Delta\omega$ can be estimated as $\Delta\omega \approx c/\sqrt{S}$ where c is sound velocity, and \sqrt{S} is an estimate to the transverse dimension. Indeed, Schwab *et al.* have done a remarkable experiment that verified the above theoretical prediction [26]. This thermal conductance quantum is independent of the types of energy carriers; it is also the same for electrons [27], even photons [28].

2.2 Calculation of transmission coefficients

When the transmission is not ideal, we must do a hard calculation for the transmission coefficient $T[\omega]$. Several approaches are possible. Such considerations also justify the Landauer formula itself. Blencowe in ref. [19] presented a derivation using elastic wave models. In this article, our emphasis will be on atomistic models. We will give an outline of a derivation using lattice models. Alternatively, the Landauer formula can be derived also from an NEGF formalism. But before doing this, we comment on the elastic models.

Elastic wave continuum models have been used extensively in connection with the universal thermal conductance [16,17,18,19,20]. This is justified on the ground that at very low temperatures, only the long-wave, low frequency acoustic phonons contribute to the thermal transport. Since the wavelengths are much larger than the lattice spacings of the materials, continuum models are good approximations. Often times, one takes a very simple scalar wave governed by the equation

$$\frac{\partial^2 \Psi}{\partial t^2} - c^2 \nabla^2 \Psi = 0, \quad (9)$$

with appropriate (von Neumann) boundary conditions. The elastic wave theories have been used to investigate the robustness of the universal thermal conductance in

various geometries including the effect of surface roughness [29,30], abrupt junctions [31,32], bends [33], and other channel shapes [34,35,36]. Many papers appear recently on scalar elastic-wave models with various geometries such as superlattices, T-junctions, stub junctions, etc [37,38,39,40,41,42,43,44,45,46,47,48,49,50].

It is important to ask the question, at what temperature do the elastic models break down? In an elastic model for a 2D channel, the dispersion relation takes the form

$$\omega^2 = (cq)^2 + bn^2, \quad n = 0, 1, 2, \dots \quad (10)$$

where c is sound velocity, q is wave number, and b is some constant. Clearly, the concept of Brillouin boundary is absent in elastic systems. Also, the optical phonons are not represented correctly. Thus the elastic models will not be correct quantitatively when $k_B T > \hbar \Delta \omega$. When the typical phonons have the wavelengths comparable to the lattice spacings of a crystal, we expect that the continuum theory breaks down. This happens when $\hbar c/a \sim k_B T$, where a is lattice constant. Alternatively, real crystals have an upper cut-off frequency, ω_{\max} , and associated Debye temperature, $T_D = \hbar \omega_{\max}/k_B$. The values of temperatures of the above estimates for real systems appear to be in the range 100 to 1000 K. It is then interesting to see a good comparison between elastic models and lattice models (e.g., carbon nanotubes) for thermal transport.

2.2.1 Scattering picture and Landauer formula

In this subsection, we give a derivation of the Landauer formula from an atomistic model of subsec. 1.1, following the steps of refs. [19,23,51,52]. First, in order to define the transmission amplitudes, we need to discuss the normal modes and the scattering problem. Let us consider only one lead as a quasi-one-dimensional system consisting of N repeating cells with periodic boundary conditions. We'll take $N \rightarrow \infty$ eventually. Due to periodicity, the displacements of the normal modes satisfy Bloch theorem, so that all the cells are oscillating in essentially the same way except a phase factor (see, e.g., ref. [53]). We write

$$u_l = \epsilon \lambda^l e^{-i\omega t}, \quad (11)$$

where u_l is a column vector for the displacements in cell l for M degrees of freedom, ϵ is the polarization vector (of dimension M) satisfying the equation

$$\left(\omega^2 I - k_{11} - \frac{1}{\lambda} k_{10} - \lambda k_{01} \right) \epsilon = 0. \quad (12)$$

The identity matrix I , the spring constant matrices for a single cell, k_{11} , k_{10} , and k_{01} , are size $M \times M$. Imposing the Born-von Karman boundary condition, $u_l = u_{l+N}$, one gets $\lambda = e^{i2\pi k/N} = e^{iqa}$, $q = 2\pi k/(aN)$; a is the lattice constant. We can choose the integer $k = -N/2, -N/2 + 1, \dots, N/2 - 1$ for the linearly independent solutions. For each k , Eq. (12) gives M eigenmodes with angular frequency $\omega_{n,k}$ and polarization vector $\epsilon_{n,k}$, where $n = 1, 2, \dots, M$ labels the branches, and k labels the wave vectors. We'll

normalize the polarization vector such that $\epsilon_{n,k}^\dagger \epsilon_{n',k} = \delta_{n,n'}$. The dagger stands for Hermitian conjugate. Note that $\epsilon_{n,k}$ in general is complex. We demand that $\epsilon_{n,k}^* = \epsilon_{n,-k}$. A particular vibrational mode is considered to be a general motion can be expressed in terms of normal mode coordinates $Q_{n,k}(t)$, as $u_l(t) = N^{-1/2} \sum_{n,k} Q_{n,k}(t) \tilde{u}_{l,n,k}$. In terms of the normal modes, the total energy of the system is

$$H_R = \frac{1}{2} \sum_{n,k} \left(|\dot{Q}_{n,k}(t)|^2 + \omega_{n,k}^2 |Q_{n,k}(t)|^2 \right). \quad (13)$$

In the derivation below, we need an expression for the group velocity $v = \partial\omega/\partial q$ in terms of the eigenvectors. This is obtained by differentiating the eigenvalue equation, (12), with respect to the wavevector q , and multiplying the resulting equation with ϵ^\dagger from left,

$$2\omega v = ia \left(\lambda \epsilon^\dagger k_{01} \epsilon - \frac{1}{\lambda} \epsilon^\dagger k_{10} \epsilon \right). \quad (14)$$

We have used the Hermitian conjugate of Eq. (12) to eliminate a term involving $\partial\epsilon/\partial q$.

In a scattering problem setting, we usually specify a frequency first, and ask the value of wavevector q for a given mode n . For this reason, we consider the normal modes as specified by

$$\tilde{u}_{l,n}(\omega) = \epsilon_n(\omega) e^{iq_n(\omega)la}. \quad (15)$$

We now introduce superscripts (α, σ) to specify the side of the leads, $\alpha = L$ or R , and the direction of energy transmission $\sigma = \pm$. We'll use the convention that energy flow into (group velocity toward) the center is '+'. The left lead and right lead can be different lattices and thus have different dispersion relations and eigenmodes. For notational simplicity, we'll omit the frequency argument, and use both (n, k) and (n, σ, ω) to specify the modes interchangeably. If a particular mode $\tilde{u}_{l,n}^{(L,+)}$ is sent from the left lead to the central region, part of it will be reflected back, and part of it will be transmitted. For the cells far away from the center, the waves take the asymptotic form

$$u_l^L = \tilde{u}_{l,n}^{(L,+)} + \sum_{n'} \tilde{u}_{l,n'}^{(L,-)} t_{n'n}^{LL}, \quad l \rightarrow -\infty \quad (16)$$

on the left lead, and

$$u_l^R = \sum_{n'} \tilde{u}_{l,n'}^{(R,-)} t_{n'n}^{RR}, \quad l \rightarrow +\infty \quad (17)$$

on the right lead. Equation (17) defines the transmission amplitude $t_{n'n}^{RL}$ at frequency ω of the mode n to mode n' on the right, while Eq. (16) defines the reflection amplitude back into mode n' . Similarly, we can send waves from the right lead to the left lead and define analogously t^{LR} and t^{RR} . From these transmission amplitudes, the total transmission, $T[\omega]$, can be calculated.

Our next task is to find a classical expression for the energy current and then to quantize the expression and

find quantum energy current. An expression for microscopic energy current can be obtained by considering the conservation of energy [9]. For a quasi-1D system, this is

$$\frac{dH_l}{dt} + I_{l+1} - I_l = 0, \quad (18)$$

where we define the local energy in cell l as

$$H_l = \frac{1}{2} (\dot{u}_l^T \dot{u}_l + u_{l-1}^T k_{01} u_l + u_l^T k_{11} u_l + u_{l+1}^T k_{10} u_l), \quad (19)$$

such that $\sum_l H_l = H_R$ (or H_L). By differentiating H_l with respect to time t and using the equation of motion, we can see that

$$I_l = \frac{1}{2} u_l^T k_{10} \dot{u}_{l-1} - \frac{1}{2} u_{l-1}^T k_{01} \dot{u}_l \quad (20)$$

satisfies the requirement. I_l is the energy current from cell $l-1$ to cell l . Expressing a general vibration as superposition of modes with amplitudes $Q_{n,k}$,

$$u_l(t) = \frac{1}{2\sqrt{N}} \sum_{n,k} Q_{n,k} \epsilon_{n,k} \lambda^l e^{-i\omega_{n,k}t} + \text{c.c.}, \quad (21)$$

where c.c. stands for complex conjugate, and substituting it into Eq. (20), and performing a time average, we obtain

$$\langle I_l \rangle = \frac{1}{4N} \sum_{n,k} i\omega_{n,k} |Q_{n,k}|^2 \epsilon_{n,k}^\dagger \left(\lambda k_{01} - \frac{1}{\lambda} k_{10} \right) \epsilon_{n,k}. \quad (22)$$

In deriving the above expression, we used the fact that the time average of $e^{i(\omega_{n,k} - \omega_{n',k'})t}$ is zero, unless $n = n'$ and $k = k'$. The expression in the brackets can be further simplified in terms of the group velocity $v_{n,k} = \partial\omega_{n,k}/\partial q$. The final expression for the classical energy current in terms of the normal mode amplitudes is

$$I = \sum_{n,k} \frac{v_{n,k}}{2aN} \omega_{n,k}^2 |Q_{n,k}|^2. \quad (23)$$

We now derive a set of constraint equations for the transmission amplitudes $t_{nn'}^{\alpha\alpha'}$ due to energy conservation. Consider an arbitrary linear combination of excitations at frequency ω with incident waves from left and right, the total vibration at lead α can be written as

$$\sum_n a_n^\alpha \tilde{u}_{l,n}^{(\alpha,+)} + \sum_{n,n',\alpha'} t_{nn'}^{\alpha\alpha'} a_{n'}^{\alpha'} \tilde{u}_{l,n}^{(\alpha,-)}. \quad (24)$$

The first term above represents the superpositions of various incident modes, while the second term contains reflected waves, as well as incident waves from the opposite side. Comparing with the definition of normal mode amplitude, we find $Q_{n,k} = \sqrt{N} a_n^\alpha$ for these n and k corresponding to incoming waves, and equal to $\sqrt{N} \sum_{n',\alpha'} t_{nn'}^{\alpha\alpha'} a_{n'}^{\alpha'}$ for these of outgoing waves. Substituting the values of $Q_{n,k}$ into Eq. (23), we find the incoming current from lead α to the center,

$$I_\alpha(\omega) = \omega^2 \sum_n \frac{v_n^\alpha}{2a\alpha} \left(|a_n^\alpha|^2 - \left| \sum_{n',\alpha'} t_{nn'}^{\alpha\alpha'} a_{n'}^{\alpha'} \right|^2 \right). \quad (25)$$

In the above formula, we have the convention that v_n^α represents the magnitude and thus is always positive. Demanding that $I_L + I_R = 0$ for any amplitudes a_n^α , we obtain

$$\mathbf{t}^\dagger \tilde{\mathbf{v}} \mathbf{t} = \tilde{\mathbf{v}}, \quad (26)$$

where \mathbf{t} is a matrix with elements $t_{nn'}^{\alpha\alpha'}$ where (α, n) are considered row index and (α', n') the column index. $\tilde{\mathbf{v}}$ is a diagonal matrix with the elements $\tilde{v}_n^\alpha = v_n^\alpha/a_\alpha$ arranged in the same order as \mathbf{t} . a_L and a_R are the lattice constants of the left and right lead, respectively. The matrix \mathbf{t} is somewhat close to be unitary, but is not. If we define $\mathcal{S} = \tilde{\mathbf{v}}^{1/2} \mathbf{t} \tilde{\mathbf{v}}^{-1/2}$, then \mathcal{S} is unitary. From $\mathcal{S} \mathcal{S}^\dagger = \mathcal{S}^\dagger \mathcal{S} = I$, we can also show that

$$\mathbf{t} \tilde{\mathbf{v}}^{-1} \mathbf{t}^\dagger = \tilde{\mathbf{v}}^{-1}. \quad (27)$$

We now discuss the quantization of the problem. First, we consider only an isolated lead with periodic boundary conditions. Let us introduce the annihilation operator in Heisenberg picture $a_{n,k}(t) = a_{n,k} e^{-i\omega_{n,k}t}$ associated with mode (n, k) and its Hermitian conjugate $a_{n,k}^\dagger(t)$ for the creation operator, satisfying the usual commutation relations, $[a_{n,k}, a_{n',k'}] = 0$, $[a_{n,k}^\dagger, a_{n',k'}^\dagger] = 0$, and $[a_{n,k}, a_{n',k'}^\dagger] = \delta_{n,n'} \delta_{k,k'}$. Then the canonical coordinate operator is

$$\hat{Q}_{n,k}(t) = \sqrt{\frac{\hbar}{2\omega_{n,k}}} \left[a_{n,k}(t) + a_{n,-k}^\dagger(t) \right], \quad (28)$$

satisfying $[\hat{Q}_{n,k}(t), \dot{\hat{Q}}_{n',k'}^\dagger(t)] = i\hbar \delta_{n,n'} \delta_{k,k'}$. Using the relation between the normal mode coordinates and the original coordinates, we can write

$$\hat{u}_l(t) = \sum_{n,k} \sqrt{\frac{\hbar}{2\omega_{n,k}N}} \epsilon_{n,k} e^{i\frac{2\pi kl}{N}} a_{n,k}(t) + \text{h.c.}, \quad (29)$$

where h.c. stands for Hermitian conjugate of the preceding term. We have $[\hat{u}_l(t), \dot{\hat{u}}_{l'}^\dagger(t)] = i\hbar I \delta_{l,l'}$, as required. We now substitute Eq. (29) into the current expression, Eq. (20), taking a time average, and using the result of Eq. (14), we get

$$\hat{I} = \frac{1}{aN} \sum_{n,k} v_{n,k} \hbar \omega_{n,k} a_{n,k}^\dagger a_{n,k}. \quad (30)$$

This is a well-known result for the energy current for a lattice [54].

For the open system with two leads and a central junction, we need to consider the two sides simultaneously even if our interest is only the current on the left lead. Specifically the creation and annihilation operators will be associated with the scattering state Eq. (16) and (17), originating from the left lead, $a_{n,k}^L$, and a similar one originating from the right lead, $a_{n,k}^R$. The general displacement operator \hat{u} is a superposition of the scattering waves similar to Eq. (24), with the number a_n^α replaced by the operator $\sqrt{\hbar/(2\omega N)} a_{n,k}^\alpha(t)$ and summed over all

modes, plus its h.c.. After substituting the operator \hat{u} into the current expression, Eq. (20), we obtain many terms, quadratic in $a_{n,k}^\alpha$ or $a_{nk}^{\alpha\dagger}$. Now at this point, great simplification can be made if we evoke nonequilibrium thermodynamic average. We assume that the scattering states are distributed according to equilibrium distribution at temperature $T_L = 1/(k_B\beta_L)$ for the mode originating from the left lead, and T_R for those originating from the right lead. This causes an asymmetry for the left moving and right moving phonon waves, thus generates a thermal current. The thermal average $\langle \dots \rangle$ can be thought of as taking the trace of the creation/annihilation operators with respect to a density matrix given by $\rho \propto e^{-\beta_L H_L - \beta_R H_R}$, with the following results

$$\langle a_{n,k}^\alpha a_{n',k'}^{\alpha'} \rangle = 0, \quad (31)$$

$$\langle a_{n,k}^\alpha \dagger a_{n',k'}^{\alpha'} \rangle = 0, \quad (32)$$

$$\langle a_{n,k}^\alpha \dagger a_{n',k'}^{\alpha'} \rangle = \delta_{n,n'} \delta_{k,k'} \delta_{\alpha,\alpha'} f_\alpha, \quad (33)$$

where f_α is the Bose-Einstein distribution function at the temperature T_α . Using the above results, Eq. (14), and with some algebra, we get, after cancelling the terms corresponding to the zero-point motions,

$$\langle I_\alpha \rangle = \sum_{k>0,n} \frac{\hbar \omega_{n,k} v_{n,k}^\alpha}{a_\alpha N_\alpha} \left[f_\alpha(\omega_{n,k}) - \sum_{n',\alpha'} |t_{nn'}^{\alpha\alpha'}|^2 f_{\alpha'}(\omega_{n,k}) \right]. \quad (34)$$

Using the properties of the matrix \mathbf{t} , Eq. (26) and (27), we can make the expression more symmetric with respect to the leads. We finally take the limit $N \rightarrow \infty$ by replacing $\sum_k v_{n,k}^\alpha / (a_\alpha N_\alpha) \dots$ by $\int d\omega / (2\pi) \dots$. We obtain the Landauer formula, Eq. (5), with the total transmission given by [52],

$$T[\omega] = \sum_{n,n'} \frac{\tilde{v}_{n'}^R}{\tilde{v}_n^L} |t_{n'n}^{RL}|^2. \quad (35)$$

The above formula has a very simple physical interpretation. The total transmission at a given frequency is a sum of all possible incoming channels n from the left and all outgoing channels n' on the right. Each term is simply the ratio of the energy current of the transmitted wave $\tilde{u}_{l,n'}^{(R,-)} t_{n'n}^{RL}$ to the incident wave $\tilde{u}_{l,n}^{(L,+)}$. Since energy must be conserved, each term cannot exceed 1.

2.2.2 Generalized eigenvalue problem

The eigen modes can be found by Eq. (11) and Eq. (12). In a standard dispersion relation calculation, one specifies a wave number q first, and then solves Eq. (12) to find various eigen frequencies. This is inconvenient for solving a scattering problem. Here we like to specify a frequency ω first, and find q and associated polarization vector ϵ . To do this [55,56,57], we rewrite Eq. (12) in a form so that

$\lambda = e^{iqa}$ becomes an eigenvalue. Let us introduce a new vector ζ the same dimension as ϵ , by $k_{10}\epsilon = \lambda\zeta$, then

$$\begin{pmatrix} \omega^2 I - k_{11} & -I \\ k_{10} & 0 \end{pmatrix} \begin{pmatrix} \epsilon \\ \zeta \end{pmatrix} = \lambda \begin{pmatrix} k_{01} & 0 \\ 0 & I \end{pmatrix} \begin{pmatrix} \epsilon \\ \zeta \end{pmatrix}, \quad (36)$$

where I is an $M \times M$ identity matrix. Equation (36) sets up a so-called generalized eigenvalue problem. Since our eigenvalue problem has a dimension of $2M$, we'll have upto $2M$ eigenvalues for λ . One can prove that the eigenvalues come in pair of inverse of each other, $\lambda_+ \lambda_- = 1$. Most of the eigenvalues represent evanescent modes, but these with $|\lambda| = 1$ represent traveling waves.

It is convenient to know the sign of the group velocity without actually calculating it. By adding a small imaginary part to ω , that is, replacing it by $\omega + i\eta$, then none of the eigenvalues λ will have modulus exactly 1. Considering η as a small perturbation, we find for the traveling waves [58]

$$|\lambda| = 1 - \eta \frac{a}{v}, \quad \eta \rightarrow 0^+. \quad (37)$$

That is, the forward moving waves with group velocity $v > 0$ have $|\lambda| < 1$. This result will be handy for constructing the surface Green's function of the lead later.

2.2.3 Scattering boundary condition method

In ref. [52], Wang *et al.* proposed a scattering boundary condition method to compute the transmission coefficient $t_{n'n}^{\alpha\alpha'}$. The method is similar but not quite the same as the mode-matching methods [59,55,60] used in electronic transport. The idea is very simple. We write down the linear equations for the center, and impose the scattering boundary condition to solve it. Let us name the supercells consistently so that the left lead will have $l = \dots, -2, -1, 0$, the center consists of 1 to N , and right lead is $N+1, N+2, \dots$. Then the equations that have not been dealt with by the leads are

$$-k_{10}^L u_{-1} + (\omega^2 - k_{00}^L) u_0 - V^{LC} u^C = 0, \quad (38)$$

$$-V^{CL} u_0 + (\omega^2 - K^C) u^C - V^{CR} u_{N+1} = 0, \quad (39)$$

$$-V^{RC} u^C + (\omega^2 - k_{00}^R) u_{N+1} - k_{01}^R u_{N+2} = 0. \quad (40)$$

We have assumed that the interactions between the center and leads reach only the first layer of the leads immediately adjacent to the center. In these equations u^C is unknown, but u_{-1} , u_0 , u_{N+1} , and u_{N+2} are set to the values given by Eqs. (16) and (17), with $t_{n'n}^{LL}$ and $t_{n'n}^{RR}$ treated as unknowns. Since the form of Eqs. (16) and (17) is only asymptotic when the evanescent modes decay to zero, we should define the center part to include sections of the periodic leads. Alternatively, we should also include the evanescent modes in the summation of n' in the boundary conditions, but they should be excluded when calculating the total transmission.

However, if the evanescent modes are omitted, we have a linear system with too many equations and few unknowns. We solve the system numerically with a singular-value-decomposition method [61], which gives a very good

approximation to the original problem when the evanescent modes can be approximated to zero.

2.2.4 Mode-matching

Ando [59], Khomyakov *et al.* [55,60], and also Ting *et al.* [62,63] gave an elegant method for computing the transmission amplitudes which we outline briefly here. The important idea is to eliminate u_{-1} and u_{N+2} in Eqs (38) to (40) so that they form a closed set of equations that can be solved uniquely. One first solves the generalized eigenvalue problem of Eq. (36), then writes a general solution as linear combination of all the modes (including the evanescent modes). We divide the modes according to $|\lambda|$; these modes with $|\lambda| < 1$ (forward or right moving waves) will be designated +, and those of $|\lambda| > 1$ (backward moving waves) as -. We add a small positive imaginary number $i\eta$ to ω so that none of the modes will have $|\lambda| = 1$ exactly. Then we can write for the perfect periodic leads

$$\begin{aligned} u_l &= \sum_{\sigma=\pm} \sum_{n=1}^{M'} \epsilon_n^\sigma \lambda_{n,\sigma}^l a_n^\sigma \\ &= E^+ \Lambda_+^l \mathbf{a}^+ + E^- \Lambda_-^l \mathbf{a}^-, \end{aligned} \quad (41)$$

where we have written in a more compact form by introducing matrices. $E^+ = (\epsilon_1^+, \epsilon_2^+, \dots)$ is an $M \times M'$ matrix formed by the column vectors of ϵ_n^+ ; similarly for E^- . Λ_\pm is an $M' \times M'$ diagonal matrix with the eigenvalues $\lambda_{n,\pm}$, while \mathbf{a}^\pm is a column vector for the amplitudes of the modes. We normalize the vectors, $(\epsilon_n^\sigma)^\dagger \epsilon_n^\sigma = 1$. If k_{01} is not singular, then $M' = M$, the number of degrees of freedom in a cell. However, if it is singular, then $M' < M$. We exclude the trivial solutions $\epsilon_n^\sigma = 0$ in Eq. (41). The solution can be split into + and - component, $u_l = u_l^+ + u_l^-$. From Eq. (41), we see that

$$\begin{aligned} u_{l+s}^+ &= E^+ \Lambda_+^{l+s} \mathbf{a}^+ \\ &= E^+ \Lambda_+^s (E^+)^{-1} E^+ \Lambda_+^l \mathbf{a}^+ \\ &= F^+(s) u_l^+, \end{aligned} \quad (42)$$

where $F^+(s) = E^+ \Lambda_+^s (E^+)^{-1}$. If $M' < M$, the matrix inverse should be interpreted as the pseudo-inverse $[(E^+)^\dagger E^+]^{-1}$. $F^-(s)$ is similarly defined.

With the F operators defined for both the left and right lead, we can eliminate u_{-1} and u_{N+2} using the equations

$$u_{-1} = F_L^+(-1) u_0^+ + F_L^-(-1) u_0^-, \quad (43)$$

$$u_0 = u_0^+ + u_0^-, \quad (44)$$

$$u_{N+2} = F_R^+(1) u_{N+1}^+ = F_R^-(1) u_{N+1}^-. \quad (45)$$

For the scattering state, there is no backward moving waves on the right, so $u_{N+1}^- = 0$. We can eliminate u_0^- in favor of u_0^+ and u_0 . With that, we move the terms involving u_0^+ to the right-hand side of Eq. (38). For each

given incident mode $u_0^+ = \epsilon_{n,L}^+$, the transmission amplitude to n' is computed by solving Eqs. (38), (39), and (40), then obtained from the n' component of a vector

$$t_{n'n}^{RL} = ((E_R^+)^{-1} u_{N+1})_{n'}. \quad (46)$$

2.2.5 Scattering and transfer matrices

Transfer matrix methods have been used for computing the transmission coefficients in quasi-one-dimensional atomic models [64,65,66,67,68,69,70] as well as continuum models [37,36]. It is efficient in that the transfer matrix can be obtained in $O(N)$ computer time where N is the size of the central region. However, if there are evanescent modes with large $|\lambda|$, the evaluation of the transfer matrix can be numerically rather unstable, particularly if N is large. There is method to overcome this problem for special cases [71].

Let \mathbf{a}_L^+ be the incoming wave amplitude vector [c.f. Eq. (41)] from the left lead, and \mathbf{a}_R^- be the incoming wave amplitude vector from the right lead, then the scattering matrix relates the incoming waves to the outgoing waves

$$\begin{pmatrix} \mathbf{a}_L^- \\ \mathbf{a}_R^+ \end{pmatrix} = \begin{pmatrix} t^{LL} & t^{LR} \\ t^{RL} & t^{RR} \end{pmatrix} \begin{pmatrix} \mathbf{a}_L^+ \\ \mathbf{a}_R^- \end{pmatrix}, \quad (47)$$

which is the \mathbf{t} matrix introduced in subsec. 2.2.1. The transfer matrix \mathcal{T} (in the eigenmode representation), on the other hand, relates the amplitudes of the modes of left lead to the right lead:

$$\begin{pmatrix} \mathbf{a}_R^+ \\ \mathbf{a}_L^- \end{pmatrix} = \begin{pmatrix} \mathcal{T}_{11} & \mathcal{T}_{12} \\ \mathcal{T}_{21} & \mathcal{T}_{22} \end{pmatrix} \begin{pmatrix} \mathbf{a}_L^+ \\ \mathbf{a}_R^- \end{pmatrix}. \quad (48)$$

It can be checked that the transmission matrix $t^{LR} = \mathcal{T}_{22}^{-1}$, or $t^{RL} = (\mathcal{T}^{-1})_{11}^{-1}$. So, knowing the transfer matrix one can deduce the transmission amplitudes. While the scattering matrix \mathbf{t} is always square, the transfer matrix \mathcal{T} can be rectangular. The matrix inverse should be interpreted as pseudo-inverse in such a case.

We assume that the system can be divided into (principal) layers or cells, labelled by an integer index l , such that only the nearest neighbors have interactions. Then the equations of motion at a fixed frequency ω are given by

$$k_{l,l-1} u_{l-1} + (k_{l,l} - \omega^2) u_l + k_{l,l+1} u_{l+1} = 0. \quad (49)$$

If the coupling matrix $k_{l,l+1}$ is not singular, we can map from the displacements of u_{l-1}, u_l to u_l, u_{l+1} ,

$$\begin{pmatrix} u_{l+1} \\ u_l \end{pmatrix} = P_l \begin{pmatrix} u_l \\ u_{l-1} \end{pmatrix} = \begin{pmatrix} k_{l,l+1}^{-1}(\omega^2 - k_{l,l}) & -k_{l,l+1}^{-1} k_{l,l-1} \\ I & 0 \end{pmatrix} \begin{pmatrix} u_l \\ u_{l-1} \end{pmatrix}. \quad (50)$$

We call P_l also the transfer matrix (or promotion matrix). The motions of the left lead and right lead can be now

related through

$$\begin{aligned} \begin{pmatrix} u_{N+2} \\ u_{N+1} \end{pmatrix} &= P(N+1:0) \begin{pmatrix} u_0 \\ u_{-1} \end{pmatrix} \\ &= P_{N+1} P_N \cdots P_1 P_0 \begin{pmatrix} u_0 \\ u_{-1} \end{pmatrix}. \end{aligned} \quad (51)$$

We note that the transfer matrix for the leads, P_l when $l < 0$ or $l > N+1$, becomes independent of l due to periodicity of the lattice; let us call them P . P has some interesting properties: $\det(P) = 1$, and the eigenvalue problem of P is essentially the same as that of Eq. (36). We can relate Eq. (51) with (48) and obtain the transmission coefficient if we relate u_l to the amplitude \mathbf{a} . This is given by Eq. (41); rewritten in matrix form, we have

$$\begin{pmatrix} u_l \\ u_{l-1} \end{pmatrix} = \begin{pmatrix} E^+ \Lambda_+^l & E^- \Lambda_-^l \\ E^+ \Lambda_+^{l-1} & E^- \Lambda_-^{l-1} \end{pmatrix} \begin{pmatrix} \mathbf{a}^+ \\ \mathbf{a}^- \end{pmatrix}. \quad (52)$$

Let us denote the transformation matrix from \mathbf{a} to $(u_l, u_{l-1})^T$ by U_L and U_R for the left and right leads, respectively, then we have $\mathcal{T} = U_R^{-1} P(N+1:0) U_L$. On the other hand, we could also use Eq. (43), (44), and (45) to eliminate u_{-1} , u_{N+2} , and solve Eq. (51) for u_{N+1} and obtain the transmission coefficient via Eq. (46).

An interesting relation exists between the eigenvalues of ‘square’ of the transfer matrix and the total transmission due to Pichard [72]. The results are first derived for the electronic transport where the scattering matrix is unitary. Since in phonon transport \mathbf{t} is not unitary, we cannot apply the formula directly. Instead, we need to work with $\mathcal{S} = \tilde{\mathbf{v}}^{1/2} \mathbf{t} \tilde{\mathbf{v}}^{-1/2}$, and replace the amplitude vector \mathbf{a} by $\mathbf{c} = \tilde{\mathbf{v}}^{1/2} \mathbf{a}$. Then we have

$$\begin{pmatrix} \mathbf{c}_L^- \\ \mathbf{c}_R^+ \end{pmatrix} = \mathcal{S} \begin{pmatrix} \mathbf{c}_L^+ \\ \mathbf{c}_R^- \end{pmatrix}. \quad (53)$$

The corresponding transfer matrix associated with \mathcal{S} is

$$\mathcal{M} = \begin{pmatrix} \tilde{v}_R^{-1/2} & 0 \\ 0 & \tilde{v}_R^{1/2} \end{pmatrix} \begin{pmatrix} \mathcal{T}_{11} & \mathcal{T}_{12} \\ \mathcal{T}_{21} & \mathcal{T}_{22} \end{pmatrix} \begin{pmatrix} \tilde{v}_L^{-1/2} & 0 \\ 0 & \tilde{v}_L^{-1/2} \end{pmatrix}. \quad (54)$$

With \mathcal{S} and \mathcal{M} we have the Piccard identity [73,74]

$$[2I + \mathcal{M}\mathcal{M}^\dagger + (\mathcal{M}\mathcal{M}^\dagger)^{-1}]^{-1} = \frac{1}{4} \begin{pmatrix} \mathcal{S}_{RL} \mathcal{S}_{RL}^\dagger & 0 \\ 0 & \mathcal{S}_{LR}^\dagger \mathcal{S}_{LR} \end{pmatrix}, \quad (55)$$

where $\mathcal{S}_{\alpha\alpha'} = \tilde{v}_\alpha^{1/2} t^{\alpha\alpha'} \tilde{v}_{\alpha'}^{-1/2}$, $\alpha = L, R$. The eigenvalues of the product $\mathcal{M}\mathcal{M}^\dagger$ are real and positive and come in pair of inverse of each other. We denote them by $\exp(\pm 2x_k)$. Taking the trace of both sides of Eq. (55), and using the fact that the total transmission $T[\omega] = \text{Tr}(\mathcal{S}_{RL} \mathcal{S}_{RL}^\dagger)$, we obtain

$$T[\omega] = \sum_k \frac{1}{\cosh^2 x_k}. \quad (56)$$

In applying the above formula, we should use a global transfer matrix $P(N+1+s:-s)$ for a sufficiently large s to ‘‘damp out’’ the contributions from evanescent modes.

2.2.6 NEGF: Caroli formula

Another efficient way of computing the transmission coefficient is through the so-called Caroli formula:

$$T[\omega] = \text{Tr}(G^r \Gamma_L G^a \Gamma_R), \quad (57)$$

where $G^r = (G^a)^\dagger$ is the retarded Green’s function for the central region, while $\Gamma_{L,R}$ describes the interaction between the leads and the central region. Caroli *et al.* first obtained a formula for the electronic transport in a slightly more restricted case [75]. Meir and Wingreen gave the above form from NEGF formalism [76]. For thermal transport, it has been derived by many authors from various perspectives [77,78,79,80,81,82,83,12,13].

In this subsection, we only discuss the relation of Eq. (57) with the surface Green’s functions. We’ll consider a derivation in sec. 3.2. The retarded Green’s function of the full linear system, including the leads, in frequency domain is given by the solution of the equation $[(\omega + i\eta)^2 I - K]G = T I$. Both K and G are (infinite) matrices indexed by the labels of atomic degrees of freedom. Partitioning the matrices according to the left, center, and right regions, as given in Eq. (2) for K , and similarly for G , we have [82,84]

$$\begin{pmatrix} (\omega + i\eta)^2 I - K^L & -V^{LC} & 0 \\ -V^{CL} & (\omega + i\eta)^2 I - K^C & -V^{CR} \\ 0 & -V^{RC} & (\omega + i\eta)^2 I - K^R \end{pmatrix} \times \begin{pmatrix} G^{LL} & G^{LC} & G^{LR} \\ G^{CL} & G^{CC} & G^{CR} \\ G^{RL} & G^{RC} & G^{RR} \end{pmatrix} = \begin{pmatrix} I & 0 & 0 \\ 0 & I & 0 \\ 0 & 0 & I \end{pmatrix}. \quad (58)$$

Considering only the three equations formed by each row of the first matrix multiplying the middle column of G matrix, we have

$$[(\omega + i\eta)^2 I - K^L] G^{LC} - V^{LC} G^{CC} = 0, \quad (59)$$

$$-V^{CL} G^{LC} + [(\omega + i\eta)^2 I - K^C] G^{CC} - V^{CR} G^{RC} = I, \quad (60)$$

$$-V^{RC} G^{CC} + [(\omega + i\eta)^2 I - K^R] G^{RC} = 0. \quad (61)$$

Introducing the retarded surface Green’s functions for the leads

$$g_\alpha^r = [(\omega + i\eta)^2 I - K^\alpha]^{-1}, \quad \alpha = L, R, \quad (62)$$

and using Eqs. (59) and (61) to eliminate G^{LC} and G^{RC} , we can express the central part of the Green’s function as

$$G^r = G^{CC} = [(\omega + i\eta)^2 I - K^C - \Sigma_L^r - \Sigma_R^r]^{-1}, \quad (63)$$

where retarded self-energy of the leads is given by

$$\Sigma_\alpha^r = V^{C\alpha} g_\alpha^r V^{\alpha C}. \quad (64)$$

G^r is the matrix entering into the Caroli formula. The Γ_α functions are given by

$$\Gamma_\alpha = i(\Sigma_\alpha^r - \Sigma_\alpha^a) = -2 \text{Im} V^{C\alpha} g_\alpha^r V^{\alpha C}. \quad (65)$$

As we can see, the transmission coefficient can be obtained if we know the surface Green’s function g_α^r . We’ll discuss the algorithms for computing the surface Green’s functions in the next section.

2.2.7 Algorithms for surface Green's functions

In an NEGF calculation for the total transmission, an important piece of code is for the computation of the Green's function of an isolated, semi-infinite lead, satisfying, e.g., for the right lead,

$$[(\omega + i\eta)^2 I - K^R] g_R^r = I, \quad (66)$$

where K^R is given by Eq. (4). In block matrix form, for the left-most column of g_R^r , we have

$$\begin{aligned} [(\omega + i\eta)^2 I - k_{00}] g_{00} - k_{01} g_{10} &= I, \\ -k_{10} g_{l-1,0} + [(\omega + i\eta)^2 I - k_{11}] g_{l,0} \\ -k_{01} g_{l+1,0} &= 0, \quad l = 1, 2, \dots \end{aligned} \quad (67)$$

In order to be consistent with the literature on surface Green's functions, we label the right lead starting from layer $l = 0$ (instead of $N + 1$ used in Sec. 2.2.3). Since the coupling from the center to the lead only reaches the 0-th layer, we only need the $M \times M$ block matrix g_{00} . Various methods have been used [85,86,87,88,89,90,91] to find g_{00} , see [58] for an recent review.

An equation can be obtained for g_{00} by considering the relation of the original system K^R and a new system with the 0-th layer removed. Similar to the derivation of Eq. (63), this gives

$$g_{00} = [(\omega + i\eta)^2 I - k_{00} - k_{01} \tilde{g} k_{10}]^{-1}, \quad (69)$$

where \tilde{g} is the surface Green's function for a system with the 0-th layer deleted, i.e., \tilde{g} is the top-left element satisfying a similar equation as Eq. (66), but with a K matrix obtained from K^R with the 0-th block row and 0-th block column deleted. If we continue this operation of removing the next layer, we see that the K matrix will not change (since it is semi-infinite and translationally invariant), we must have

$$\tilde{g} = [(\omega + i\eta)^2 I - k_{11} - k_{01} \tilde{g} k_{10}]^{-1}. \quad (70)$$

The above equation can be iterated starting from $\tilde{g} = 0$. This is known as simple iteration method [58]. However, such iterations converge slowly. After i iterations, the result is equivalent to a truncated system of finite length of i layers.

A more efficient and popular method is that of López Sancho *et al.* [88], which doubles the number of layers in each iteration, i.e., after i iterations, the effect of 2^i layers is taken into account. We refer to ref. [88] for its derivation. Here we give a pseudo-code for such an algorithm. The left arrow ' \leftarrow ' below denotes assignment, ϵ is an error tolerance, and $|\cdot|$ stands for some matrix norm.

```

s ← k00
e ← k11
α ← k01
do {
  g ← [(ω + iη)2I - e]-1
  β ← αT

```

```

s ← s + αgβ
e ← e + αgβ + βgα
α ← αgα
} while (|α| > ε)
g00 ← [(ω + iη)2I - s]-1.

```

The most accurate and perhaps also the fastest methods [85,89,90,91] are based on the solution of the generalized eigenvalue problem, Eq. (36). We notice that $g_{l,0}$ and the general displacement u_l satisfy exactly the same equation, for $l > 0$. Thus, we can express the solution of $g_{l,0}$ in the general form of Eq. (41). However, since $g_{l,0}$ must be finite in the limit $l \rightarrow +\infty$, we can only have the decay modes (+ components) with $|\lambda| < 1$. In particular, Eq. (42) is also valid for $g_{l,0}$, that is,

$$g_{l+s,0} = F^+(s) g_{l,0}, \quad F^+(s) = E^+ \Lambda_+^s (E^+)^{-1}. \quad (71)$$

Substituting this result for $l = 0, s = 1$ into Eq. (67), we can solve for g_{00} explicitly as

$$g_{00} = [(\omega + i\eta)^2 I - k_{00} - k_{01} F^+(1)]^{-1}. \quad (72)$$

The eigenvalue problem and matrix inverses all have $O(M^3)$ in computational complexity. We note that when constructing the F^+ matrix, we need to include all the $|\lambda| < 1$ modes, including these with $\lambda = 0$ when k_{01} is singular. The surface Green's function of the left lead can be computed by the same routine by first inverting the matrix indices, applying the algorithm, and then inverting g_{00} back again.

2.2.8 Relation between scattering picture and NEGF

The results for the transmission coefficient from the scattering picture, Eq. (35), and the Caroli formula, Eq. (57), look quite different. It is shown explicitly in ref. [60] that they are completely equivalent. This can be done by first solving formally the mode-matching problem discussed in sec. 2.2.4 in terms of Green's function, given

$$u_{N+1} = G_{N+1,0} Q_0 \epsilon_{n,L}^+, \quad (73)$$

$$Q_0 = k_{10}^L [F_L^+(-1) - F_L^-(-1)]. \quad (74)$$

The Green's function in the above formula is the top-right corner block of G^{RL} in Eq. (58), which is related to the central part Green's function G^r by

$$G_{N+1,0} = g_{R,00}^r V^{RC} G^r V^{CL} g_{L,00}^r. \quad (75)$$

We can relate Q_0 with the surface Green's functions of the leads, and relate group velocities to self-energies, and eventually arrive at [60]

$$t_{n'n}^{RL} = i2\omega \left[(E_R^+)^{-1} G_{N+1,0} ((E_L^-)^T)^{-1} \right]_{n'n} \tilde{v}_n^L. \quad (76)$$

We can think of this result as the Fisher-Lee relation [92] for the ballistic phonon transport.

To illustrate the methods, we consider a defect model of carbon nanotube where the mass of one of the carbon

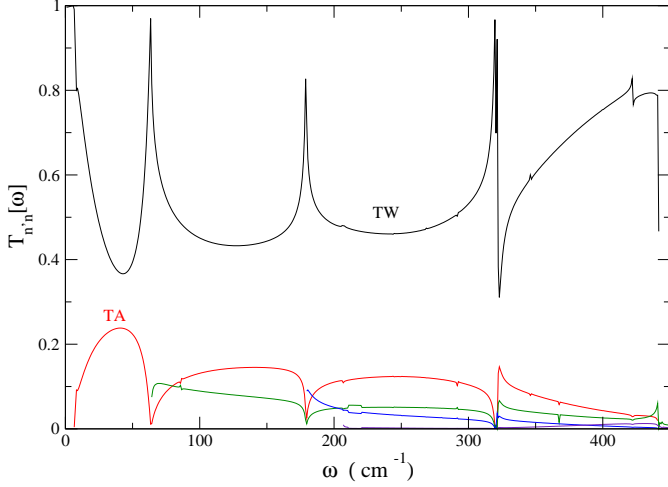


Fig. 2. Partial transmission $T_{n'n}[\omega]$ of the TW (twist) mode for a (8,0) carbon nanotube with a pinning defect site. The curve with label TW is from TW to TW, and that with TA is from TW to TA, other unlabelled curves correspond to TW to optical modes. The values given are sum of the two degenerate modes of TA or optical modes.

atom is set to infinite, creating a strong pinning at the site. The force constants are obtained from Brenner potential [93]; starting with a perfect nanotube structure, the values of rows and columns of the K matrix corresponding to the defect atom are set to 0. Unlike some of the other defects [81,94,95], such pinning has a strong effect to the low frequency transmissions due to broken translational invariance. It also produces strong mode mixings. In Fig. 2, we show the partial transmission, defined as, $T_{n'n}[\omega] = |t_{n'n}^{RL}|^2 \tilde{v}_n^R / \tilde{v}_n^L$. This quantity can be computed by the mode-matching method of sec. 2.2.4 or by Eq. (76). We observe that substantial fraction of the twist (TW) mode vibration is converted into transverse acoustic (TA) modes and other optical modes. Due to symmetric reason, the longitudinal mode is not excited and has zero transmission. The peaks in the TW to TW transmission are associated with the presence of an optical mode with zero group velocity.

2.2.9 Transmission from molecular dynamics

Schelling *et al.* proposed a MD method to compute the transmission coefficient [96,97,98,99,94]. The idea is to send a wavepacket localized both in real space and momentum space, and to measure the fraction of energy transmitted from one lead to the other. The method is applied to semi-conductor interfaces and nanowires, grain boundaries, as well as carbon nanotubes with point defects. If the amplitudes of the waves are small enough, the results are effectively the same as that of lattice dynamics or NEGF. Due to limited resolution in both space and time in MD, the results are typically less accurate. However, the simulation can give a good visual presentation of the phonon dynamics.

The initial wavepacket can be constructed either in real space or in momentum space. For example, we can consider the superposition of eigenmodes of different frequencies,

$$u_l(t) = \int_{-\infty}^{+\infty} a_n(\omega) \epsilon_{n,L}^+(\omega) \lambda_{n,L}^{l-l_0}(\omega) e^{-i\omega t} \frac{d\omega}{2\pi} + c.c. \quad (77)$$

If we choose $a_n(\omega) \propto e^{-(\omega-\omega_0)^2/(2\sigma^2)}$, we'll have a wavepacket centered around l_0 at $t = 0$ in real space with a spread of order \tilde{v}_n/σ lattice spacings.

2.3 Dimension crossover, etc.

In this section, we mention some of the work that has been done for ballistic phonon transport, using the techniques mentioned earlier. One interesting aspect of ballistic transport is the dimension effect. For quasi-one-dimensional systems, at sufficiently low temperatures, we expect that the conductance depends on temperature linearly, $\sigma \propto T$. Calculations on carbon nanotubes and graphene strips [100,101] confirm this expectation. It is interesting to know, but to our knowledge not answered, how the 1D behavior crosses over to a full 2D behavior. Naively, we expect that $\sigma \propto T^d$, where d is the dimensionality. In two dimensions, this is not the case, but it is given by $T^{3/2}$ [21,102]. This is because that one of the acoustic branch has a dispersion relation that is quartic in the wavevector. In ref. [103], diameter dependence of silicon nanowires is studied using NEGF method. It is found that, as the diameter increases, the effective exponent increases from 1 to 3, where $d = 3$ being the bulk value. Interfaces [104] and atomistic junction systems [105,106] have been studied. The effect to thermal current of Stone-Wales defects in graphene nanoribbons is studied in [107]; and the phonon transmission through defects in carbon nanotubes using first principles force constants is studied in [108]. In ref. [109] Landauer-like formula for thermal transport through a mesoscopic weak link is given.

3 Nonlinear effects in thermal transport

3.1 Phenomenological treatment of nonlinear interactions: effective transmission

If we take a short piece of quasi-one-dimensional material, such as a carbon nanotube, with an ideal lead-system contact and ignoring nonlinearity, the thermal energy transmission is given by the Landauer formula with the transmission coefficient given by Eq. (7). Each mode n is described by a simple rectangular function, $T_n[\omega] = 1$ for the frequency ω within the phonon band of the n -th branch, and $T_n[\omega] = 0$ outside the band. However, this picture breaks down if the system is long in comparison with the phonon mean free path. In ref. [110] (and also [70]), a phenomenological description of the effect of finite phonon

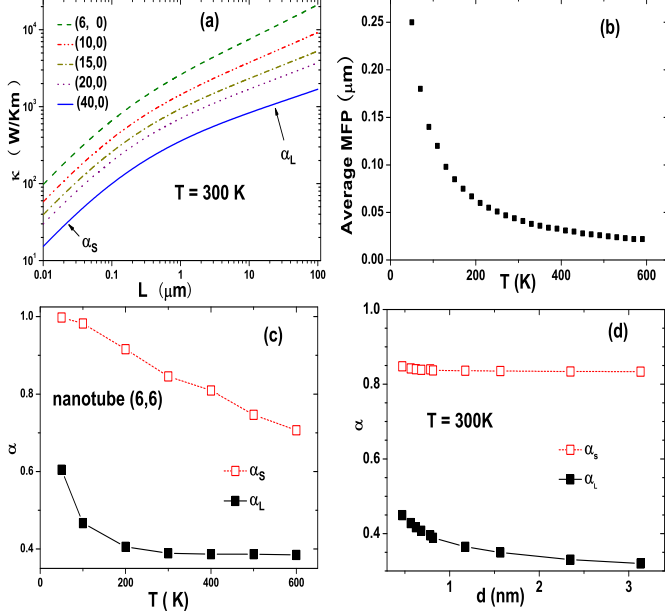


Fig. 3. Carbon nanotube thermal transport in ballistic-diffusive regimes: (a) Length dependence of thermal conductivity for different chirality SWCNTs at 300 K; (b) Average mean free path for nanotube (6,6) as a function of temperature; (c) Change of the effective power-law exponents for short and long CNTs with temperature; (d) Change of the exponents with diameter. From ref. [110].

mean free path is taken into account in analogy to the electron transport [111]:

$$T_n[\omega] = (1 + L/\ell_n(\omega))^{-1}, \quad (78)$$

where $\ell_n(\omega)$ is the mean free path of phonons of mode n with frequency ω (A quite different form, $1/T[\omega] \propto (\omega - \omega_0)^2 + d^2$, was used in ref. [112], which cannot account for the nonlinear effect). This formula interpolates between the ballistic transport and diffusive transport. When $\ell_n \gg L$ we obtain the Landauer formula, while in the opposite limit, we reproduce the well-known Debye-Peierls formula for the thermal conductivity.

The mean free path is related to the phonon relaxation time by $\ell_n = \tau_n v_n$, where v_n is phonon group velocity. The relaxation time can be obtained by considering the detailed scattering mechanisms, such as Umklapp processes, defect and boundary scatterings [113,114,115,116,117,118,119,120]. When detailed structure and nonlinear information are put in, Eq. (78) should be able to give quantitatively correct predictions. In ref. [110], a phenomenological expression $\ell \approx A/(\omega^2 T)$ is used for a calculation of carbon nanotube. The divergence thermal conductivity exponents are defined by $\kappa \propto L^{\alpha_S}$ or L^{α_L} for short and long carbon nanotubes. As shown in Fig. 3, at a fixed temperature, the thermal conductivity grows with system sizes with a large exponent for short nanotubes and reduces to a smaller exponent for much longer tubes. We notice that purely diffusive behavior is not observed even for systems as long as 100 μm .

3.2 Nonequilibrium Green's function method

The nonequilibrium Green's function (NEGF) method is an elegant and powerful method to treat nonequilibrium and interacting systems in a rigorous way. Its root is from quantum field theory. Some of the early formulations are by Schwinger [121], Kadanoff and Baym [122], and perhaps most significantly by Keldysh [123]. The books of refs. [124,125] contain some interesting historical aspects of the developments. The Keldysh diagrammatic expansion method is also generalized to cases of arbitrary (correlated) initial states [126]. Meir et al. [76,127] applied the technique to electronic transport through junctions. We recommend the books by Datta [111] and Haug and Jauho [128] for some necessary backgrounds in this topic. The application of NEGF method to thermal transport is relatively recent. In refs. [77,129,81], ballistic transport is treated. However, the real strength of the NEGF method is its ability to handle nonlinear interactions rigorously, at least in principle [12,13,130,131,83].

3.2.1 Definitions of the Green's functions and their relations

In NEGF approach, it is convenient and also necessary to introduce several different versions of the Green's functions. We will start with the definition of six Green's functions [132,133]:

$$G^r(t, t') = -i\theta(t - t')\langle[u(t), u(t')^T]\rangle, \quad (79)$$

$$G^a(t, t') = i\theta(t' - t)\langle[u(t), u(t')^T]\rangle, \quad (80)$$

$$G^>(t, t') = -i\langle u(t)u(t')^T \rangle, \quad (81)$$

$$G^<(t, t') = -i\langle u(t')u(t)^T \rangle^T, \quad (82)$$

$$G^t(t, t') = \theta(t - t')G^>(t, t') + \theta(t' - t)G^<(t, t'), \quad (83)$$

$$G^{\bar{t}}(t, t') = \theta(t' - t)G^>(t, t') + \theta(t - t')G^<(t, t'). \quad (84)$$

They are known as retarded, advanced, greater, lesser, time-ordered, and anti-time ordered Green's functions, respectively. $u(t)$ is a column vector of the particle displacement in Heisenberg picture. The step function $\theta(t) = 1$ if $t \geq 0$ and 0 if $t < 0$. The notation $\langle[A, B^T]\rangle$ represents a matrix and should be interpreted as $\langle AB^T \rangle - \langle BA^T \rangle^T$. To avoid the \hbar floating around, we have set $\hbar = 1$ in this section.

In equilibrium or nonequilibrium steady states, the Green's functions depend only on the difference in time, $G^r(t, t') = G^r(t - t')$. The Fourier transform of $G^r(t - t') = G^r(t, t')$ is defined as

$$G^r[\omega] = \int_{-\infty}^{+\infty} G^r(t) e^{i\omega t} dt. \quad (85)$$

Note that we use square brackets to delimit the argument for the Green's functions in frequency domain. The following linear relations hold in both frequency and time domains from the basic definitions:

$$G^r - G^a = G^> - G^<, \quad (86)$$

$$G^t + G^{\bar{t}} = G^> + G^<, \quad (87)$$

$$G^t - G^{\bar{t}} = G^r + G^a. \quad (88)$$

Also, the relations $G^r = G^t - G^<$ and $G^a = G^< - G^{\bar{t}}$ are useful. Out of the six Green's functions, only three of them are linearly independent. However, in systems with time translational invariance, the functions G^r and G^a are Hermitian conjugate of one other:

$$G^a[\omega] = (G^r[\omega])^\dagger. \quad (89)$$

So in general nonequilibrium steady-state situations, only two of them are independent. We consider them to be G^r and $G^<$, but other choices are possible. There are other relations in the frequency domain as well:

$$G^<[\omega]^\dagger = -G^<[\omega], \quad (90)$$

$$G^r[-\omega] = G^r[\omega]^*, \quad (91)$$

$$G^<[-\omega] = G^>[\omega]^T = -G^<[\omega]^* + G^r[\omega]^T - G^r[\omega]^*. \quad (92)$$

The last two equations show that we only need to compute the positive frequency part of the functions.

Equations (86) to (92) are generally valid for nonequilibrium steady states. In thermal equilibrium, there is an additional equation relating G^r and $G^<$:

$$G^<[\omega] = f(\omega) \left(G^r[\omega] - G^a[\omega] \right), \quad (93)$$

where $f(\omega)$ is the Bose-Einstein distribution function at temperature T . Equation (93) is obtained by writing the Green's functions as a sum of energy eigenstates (known as the Lehmann representation, see, e.g., ref. [134]). In equilibrium, we also have $G^>[\omega] = e^{\beta\omega} G^<[\omega]$. Thus in equilibrium, there is only one independent Green's function; we take it to be G^r .

The last definition of Green's functions is the contour-ordered Green's function, which is the most convenient entity for a diagrammatic expansion. It is defined by

$$G(\tau, \tau') = -i \langle T_\tau u(\tau) u(\tau')^T \rangle, \quad (94)$$

where the variable τ is on a Keldysh contour from $-\infty$ to $+\infty$ and back from $+\infty$ to $-\infty$. The contour-ordered Green's function includes four different Green's functions given earlier:

$$G^{\sigma\sigma'}(t, t') = \lim_{\epsilon \rightarrow 0^+} G(t + i\epsilon\sigma, t' + i\epsilon\sigma'), \quad \sigma = \pm(1). \quad (95)$$

We have introduced a branch index σ , such that $\tau = t + i\epsilon\sigma$. This is purely a book-keeping device to indicate the branch that the τ variable is at, $\sigma = +1$ means τ is at the $-\infty$ to $+\infty$ branch, while $\sigma = -1$ means τ is at the returning branch. With this notation, we can identify that $G^{++} = G^t$, $G^{--} = G^{\bar{t}}$, $G^{+-} = G^<$, and $G^{-+} = G^>$, or in matrix form

$$G(\tau, \tau') \rightarrow \begin{pmatrix} G^t & G^< \\ G^> & G^{\bar{t}} \end{pmatrix}. \quad (96)$$

In dealing with the contour-ordered Green's functions, we often encounter convolution of the form

$$B(\tau, \tau') = \int d\tau_1 \int d\tau_2 \cdots A_1(\tau, \tau_1) A_2(\tau_1, \tau_2) \cdots A_n(\tau_{n-1}, \tau'). \quad (97)$$

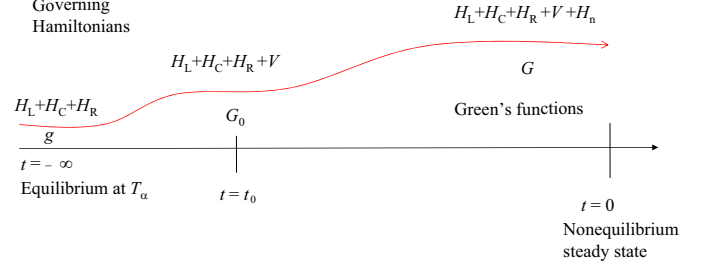


Fig. 4. A schematic to illustrate the two adiabatic switch-ons. From ref. [13].

This form of expression can be easily translated into the retarded and lesser Green's functions in frequency domain by the Langreth theorem as [135,128,136]

$$B^r[\omega] = A_1^r[\omega] A_2^r[\omega] \cdots A_n^r[\omega], \quad n = 2, 3, \cdots \quad (98)$$

$$B^<[\omega] = A_1^r[\omega] \cdots A_{n-1}^r[\omega] A_n^<[\omega] + A_1^r[\omega] \cdots A_{n-2}^r[\omega] A_{n-1}^<[\omega] A_n^a[\omega] + \cdots + A_1^<[\omega] A_2^a[\omega] \cdots A_{n-1}^a[\omega] A_n^a[\omega]. \quad (99)$$

3.2.2 Green's functions of the free leads

We will adopt the following notations, the Green's functions of the semi-infinite, equilibrium free left or right lead will be denoted g , while the ballistic system of nonequilibrium, noninteracting Green's functions will be denoted G_0 , and the full interacting system will be denoted by G . Their relations are shown schematically in Fig. 4 through two adiabatic switch-on's of the interactions. In this subsection, we discuss the Green's function of the leads. To make a connection with the Green's functions discussed in sec. 2.2.6, we consider the equations of motion of the Green's functions of the right lead. By differentiating the definitions of various Green's functions with respect to time t twice, using the Heisenberg equation of motion of any dynamic variable $A(t)$ of the right lead,

$$i \frac{dA(t)}{dt} = [A(t), H_R], \quad (100)$$

we can obtain the following set of equations,

$$\frac{\partial^2 g^{r,a,t}(t, t')}{\partial t^2} + K^R g^{r,a,t}(t, t') = -I\delta(t - t'), \quad (101)$$

$$\frac{\partial^2 g^{\bar{t}}(t, t')}{\partial t^2} + K^R g^{\bar{t}}(t, t') = I\delta(t - t'), \quad (102)$$

$$\frac{\partial^2 g^{<, >}(t, t')}{\partial t^2} + K^R g^{<, >}(t, t') = 0. \quad (103)$$

We can also give an equation for the contour ordered version,

$$\frac{\partial^2 g(\tau, \tau')}{\partial \tau^2} + K^R g(\tau, \tau') = -I\delta(\tau, \tau'), \quad (104)$$

where the τ variable takes values on the Keldysh contour. The contour ordered version is related to the ordinary

Green's functions through Eq. (96). In order to be consistent with the equations for g^t and $g^{\bar{t}}$, we must define a generalized δ -function on the contour as

$$\delta(\tau, \tau') \rightarrow \sigma \delta_{\sigma, \sigma'} \delta(t - t'). \quad (105)$$

Solutions to these differential equations can be obtained by Fourier transform. For example, we have

$$(\omega^2 - K^R) g^{r, a, t}[\omega] = I. \quad (106)$$

Although g^r , g^a , and g^t satisfy the same equation, their solutions are clearly different. They have different boundary conditions. The correct choice for the retarded Green's function g^r is

$$g^r[\omega] = [(\omega + i\eta)^2 - K^R]^{-1}, \quad (107)$$

where η is an infinitesimal positive quantity to single out the correct path around the poles when performing an inverse Fourier transform, such that $g^r(t) = 0$ for $t < 0$. Other Green's functions can be obtained through the general relations among the Green's functions, e.g., $g^<[\omega] = f(\omega)(g^r[\omega] - g^a[\omega])$.

3.2.3 Green's function G_0 and G

To compute the Green's functions of the nonequilibrium and interacting systems, we need to use perturbation theory and the concept of adiabatic switch-on. We can think of two adiabatic switch-on's as illustrated in Fig. 4. We imagine that at $t = -\infty$ the system has three decoupled regions, each at separate temperatures, T_L , T_C , and T_R . The couplings between the regions and the nonlinear interactions are turned off. The equilibrium Green's functions g^α at temperature T_α are known and take the form of Eq. (107). The couplings V^{LC} and V^{CR} are then turned on slowly, and a steady state of the linear system is established at some time $t_0 \ll 0$. For this linear problem, the result does not depend on T_C ; the initial condition of the finite center part is forgotten. Finally, the nonlinear interaction V_n is turned on, and at time $t = 0$, a nonequilibrium steady state is established.

The density matrices at time $t = -\infty$, t_0 , and $t = 0$ are related in the following way in the (respective) interaction pictures:

$$\rho(t_0) = S_0(t_0, -\infty)\rho(-\infty)S_0(-\infty, t_0), \quad (108)$$

$$S_0(t, t') = \mathcal{T} e^{-i \int_{t'}^t V(t'') dt''}, \quad (109)$$

$$\rho(0) = S(0, t_0)\rho(t_0)S(t_0, 0), \quad (110)$$

$$S(t, t') = \mathcal{T} e^{-i \int_{t'}^t V_n(t'') dt''}, \quad (111)$$

where \mathcal{T} is the time-order operator (assuming $t > t'$).

The contour-ordered Green's function can be obtained by a perturbation expansion of the interaction picture evolution operators (scattering matrix operators) and is expressed as:

$$G_0(\tau, \tau') = -i \langle \mathcal{T}_\tau u(\tau) u^T(\tau') e^{-i \int V(\tau'') d\tau''} \rangle_g, \quad (112)$$

$$G(\tau, \tau') = -i \langle \mathcal{T}_\tau u(\tau) u^T(\tau') e^{-i \int V_n(\tau'') d\tau''} \rangle_{G_0}, \quad (113)$$

where in Eq. (112) the unperturbed system is the uncoupled system with Green's function g , while in Eq. (113) we make perturbative expansion from G_0 . Since the coupling V is quadratic, its expansion leads to exact results, e.g., Dyson equation for the central part of variables (dropping the superscript CC),

$$G_0(\tau, \tau') = g^C(\tau, \tau') + \int d\tau_1 d\tau_2 g^C(\tau, \tau_1) \Sigma(\tau_1, \tau_2) G_0(\tau_2, \tau'), \quad (114)$$

where the self-energy due to linear interactions with the leads is

$$\Sigma(\tau_1, \tau_2) = V^{CL} g^L(\tau_1, \tau_2) V^{LC} + V^{CR} g^R(\tau_1, \tau_2) V^{RC}. \quad (115)$$

Thus, the Green's function G_0 can be expressed in terms of g exactly. Using the Langreth theorem discussed at the end of Sec. 3.2.1, the contour ordered Dyson equation gives two independent equations, the retarded version has solution identical to Eq. (63), while the lesser component can be solved to given [128]

$$G_0^<[\omega] = G_0^r[\omega] \Sigma^<[\omega] G_0^a[\omega]. \quad (116)$$

However, for the nonlinear problem of the second expansion, we need to use the machinery of Feynman diagrammatic technique [137,138,139]. Since the nonlinear interactions depend on the displacement u^C , we only need to consider the Green's functions G^{CC} . By expanding the exponential in Eq. (113), a series in the nonlinear interaction strength is obtained. The Feynman diagrams generated here are identical to the field theories of ϕ^3 and ϕ^4 [140], and are similar to that in refs. [141,142,143] for phonon retarded self-energies. Since the structure of the diagrammatic expansion of the contour ordered Green's functions is identical to the standard ground state ($T = 0$) expansion for the time-ordered Green's function, the Wick's theorem [138] is also applicable here. The result of each term in the expansion can be expressed as product of G_0 .

The expansion contains connected as well as disconnected Feynman diagrams. The disconnected diagrams are constant in time (not necessarily zero), and give rise to a thermal expansion effect. We can show that these diagrams do not contribute to the thermal transport, as they are proportional to $\delta(\omega)$ in the frequency domain. The thermal current formula has a factor of ω which makes it zero. The connected part of the Green's function satisfies a similar contour-ordered Dyson equation [133] relating G_c to G_0 through a nonlinear self-energy Σ_n :

$$G_c(\tau, \tau') = G_0(\tau, \tau') + \int d\tau_1 d\tau_2 G_0(\tau, \tau_1) \Sigma_n(\tau_1, \tau_2) G_c(\tau_2, \tau'). \quad (117)$$

In ordinary Green's functions and in frequency domain (ω argument suppressed), the above Dyson equation has solutions [128]:

$$G_c^r = ((\omega + i\eta)^2 I - K^C - \Sigma^r - \Sigma_n^r)^{-1}, \quad (118)$$

$$G_c^< = G_c^r (\Sigma^< + \Sigma_n^<) G_c^a. \quad (119)$$

The Eq. (119) is known as the Keldysh equation. The connected part of the Green's function G_c is needed to

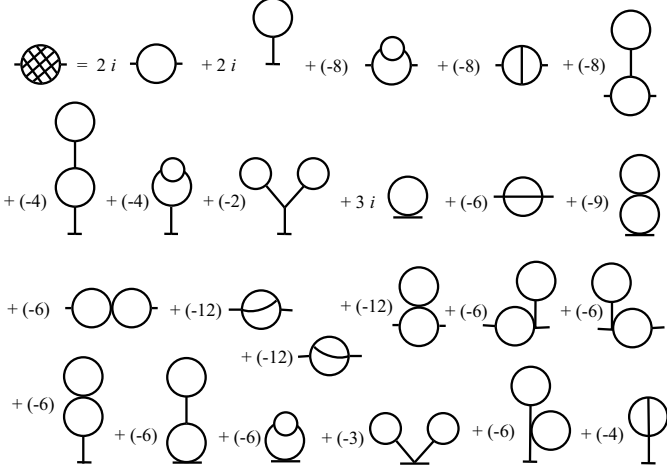


Fig. 5. The Feynman diagrams for nonlinear self-energy Σ_n with the prefactors for graphs of cubic and quartic interactions to second order in \hbar . From ref. [13].

compute the heat current. The extra subscript c will be dropped from this point.

3.2.4 Equation of motion method

An alternative method to obtain the Green's functions of interacting systems is through the equation of motion of the Green's functions. The equations of motion for various Green's functions may be used as a starting point to form mean-field type approximations. In ref. [144] the equation of motion for the nonequilibrium Green's function is justified from the Keldysh formalism, so the two approaches are completely equivalent.

It is convenient to work directly on the contour ordered Green's functions. To represent the ordering along the Keldysh contour, we introduce a generalized θ -function [145], $\theta(\tau, \tau')$, which is defined to be 1 if τ is later than τ' along the contour and 0 otherwise. Its derivative along the contour is the generalized δ -function,

$$\delta(\tau, \tau') = \frac{\partial \theta(\tau, \tau')}{\partial \tau}. \quad (120)$$

The generalized δ -function is related to its (σ, σ') components by Eq. (105). The retarded, advanced, and time-ordered components of $\delta(\tau, \tau')$ is the same as the ordinary $\delta(t-t')$, lesser and greater component is 0, while anti-time-ordered component is $-\delta(t-t')$. We also need to generalize the canonical commutation relation on the contour, as

$$\left[u_j(\tau), \frac{d}{d\tau} u_l(\tau) \right] = i \delta_{jl}. \quad (121)$$

Similarly, we also generalize the Heisenberg equation of motion,

$$\frac{dA(\tau)}{d\tau} = i[H(\tau), A(\tau)]. \quad (122)$$

Equations (121) and (122) are the same as the usual canonical commutation relation and the Heisenberg equation of

motion on the upper branch ($-\infty$ to ∞) of the Keldysh contour; but on the lower return branch, they are the time-reversed version of the equations (since $d\tau = \sigma dt$).

We first consider the linear case, $V_n = 0$. If we view the system as a whole, the contour ordered Green's function satisfies

$$-\frac{\partial^2 G_0(\tau, \tau')}{\partial \tau^2} - K G_0(\tau, \tau') = I \delta(\tau, \tau'). \quad (123)$$

This is obtained from taking derivatives twice to the definition of the contour-ordered Green's function, and using Eqs. (120) and (121). If we partition the matrix G_0 to the submatrices $G_0^{\alpha, \alpha'}$, $\alpha, \alpha' = L, C, R$, and similarly for K , we can obtain an equation similar in structure to Eq. (58) with ω^2 replaced by $-I \frac{\partial^2}{\partial \tau^2}$ and I by $I \delta(\tau, \tau')$ on the right-hand side of Eq. (58). Using a similar solution technique, we can solve for the contour-ordered nonequilibrium Green's functions

$$G_0^{LC}(\tau, \tau') = \int d\tau'' g^L(\tau, \tau'') V^{LC} G_0^{CC}(\tau'', \tau'), \quad (124)$$

$$G_0^{CC}(\tau, \tau') = g^C(\tau, \tau') + \int d\tau_1 \int d\tau_2 g^C(\tau, \tau_1) \Sigma(\tau_1, \tau_2) G_0^{CC}(\tau_2, \tau'). \quad (125)$$

The first of the above equations relates the central part of the Green's functions to the lead-center Green's function, which, it turns out, is also valid when the nonlinear interaction in the center is nonzero. The second equation is the Dyson equation relating the free leads to coupled linear system. The self-energy $\Sigma(\tau_1, \tau_2)$ is given by Eq. (115).

For the expansion of the Green's function G in terms of G_0 , we need to define a general n -point contour-ordered Green's function as

$$G_{j_1, j_2, \dots, j_n}^{\alpha_1, \alpha_2, \dots, \alpha_n}(\tau_1, \tau_2, \dots, \tau_n) = -i \langle \mathcal{T}_\tau u_{j_1}^{\alpha_1}(\tau_1) u_{j_2}^{\alpha_2}(\tau_2) \dots u_{j_n}^{\alpha_n}(\tau_n) \rangle. \quad (126)$$

The index $\alpha = L, C, R$ labels the region, j labels the degrees of freedom in that region, and τ is the contour variable. The function is symmetric with respect to simultaneous permutations of the triplet (α, j, τ) .

We can write the interactions in a more symmetric form, e.g., for the cubic term,

$$\int V_n(\tau) d\tau = \frac{1}{3} \sum_{ijk} \int \int \int T_{ijk}(\tau, \tau', \tau'') u_i^C(\tau) u_j^C(\tau') u_k^C(\tau'') d\tau d\tau' d\tau''. \quad (127)$$

Since the contour integral is $\int d\tau = \sum_\sigma \sigma \int_{-\infty}^{+\infty} dt$, we must define

$$T_{ijk}(\tau, \tau', \tau'') = T_{ijk} \delta(\tau, \tau') \delta(\tau, \tau'') \rightarrow T_{ijk} \sigma^l \delta_{\sigma, \sigma'} \delta(t-t') \sigma'' \delta_{\sigma, \sigma''} \delta(t-t''). \quad (128)$$

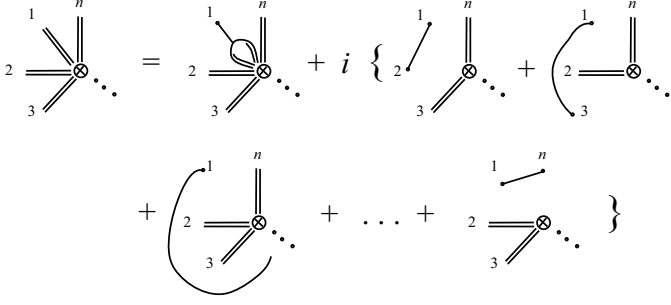


Fig. 6. Recursive expansion rule for Green's functions. A vertex with n double lines denotes an n -point Green's function. The single line denotes G_0 . A single-line three-terminal vertex is associated with $T(\tau, \tau', \tau'')$. From ref. [13].

We now consider the equation of motion of the central part Green's function G^{CC} when there is a cubic nonlinear interaction. Differentiating the Green's function with respect to τ twice, using the Heisenberg equation of motion (on the contour τ), we get

$$\begin{aligned} \frac{\partial^2 G_{jl}^{CC}(\tau, \tau')}{\partial \tau'^2} + \sum_k G_{jk}^{CC}(\tau, \tau') K_{kl}^C &= -\delta_{jl} \delta(\tau, \tau') \\ &- \sum_k G_{jk}^{CL}(\tau, \tau') V_{kl}^{LC} - \sum_k G_{jk}^{CR}(\tau, \tau') V_{kl}^{RC} \\ &- \sum_{ik} \int \int G_{jik}^{CCC}(\tau, \tau_1, \tau_2) T_{ikl}(\tau_1, \tau_2, \tau') d\tau_1 d\tau_2. \end{aligned} \quad (129)$$

The Green's functions G^{CL} and G^{CR} can be eliminated in favor of G^{CC} through (transpose of) Eq. (124). Then the differential-integral equation for G^{CC} can be solved in terms of G^{CCC} and G_0^{CC} with the help of Eq. (123). We obtain

$$\begin{aligned} G_{jl}^{CC}(\tau, \tau') &= G_{0,jl}^{CC}(\tau, \tau') + \sum_{ikm} \int \int \int G_{0,ji}^{CC}(\tau, \tau_1) \\ &T_{ikm}(\tau_1, \tau_2, \tau_3) G_{kml}^{CCC}(\tau_2, \tau_3, \tau') d\tau_1 d\tau_2 d\tau_3. \end{aligned} \quad (130)$$

This equation can be represented by a diagram. Since G^{CC} is related to a three-point Green's function, we also need the equation of motion of G^{CCC} . We can derive general rules [13] for n -point Green's functions, summarized as follows (as shown in Fig. 6):

(1) Replace leg 1 by inserting a nonlinear coupling $T(\tau, \tau', \tau'')$ such that the outer leg is immediately connected with G_0 while the other two terminals increase the order of the Green's function by 1. Quartic interaction is similar, but the process will increase the order by 2.

(2) Add imaginary unit i times a sum of the $n-1$ graphs formed by pairing each leg with leg 1 and connecting with the propagator G_0 , multiplied by a $(n-2)$ order remaining Green's function.

(3) Symmetrize the graphs, if desired, i.e., do steps (1) and (2) for every leg, 1, 2, \dots , n , add them up, and then divide by n .

These rules can be programmed with a symbolic language such as MATHEMATICA. The results are identical

to the usual expansion of $\exp[-i \int V_n(\tau) d\tau]$ and applying the Wick theorem.

3.2.5 Heat current and conductance

The formalism discussed above offers us computational method for the Green's functions, but the most important quantity to calculate in thermal transport is the heat current. In this subsection, we discuss the relationship between the Green's functions and heat current or thermal conductance. The derivation of heat current formula is similar to that of electron current in [76,128]. For interacting phonon systems, this has been carried out in [12,13,130,83].

The average rate of energy decrease in the left lead is the current flow from the left lead to the central region,

$$I_L = -\langle \dot{H}_L(t) \rangle. \quad (131)$$

In steady state, energy conservation means that $I_L + I_R = 0$. Using the Heisenberg equation of motion, we obtain, at $t=0$, $I_L = \langle (\dot{u}^L)^T V^{LC} u^C \rangle$. The expectation value can be expressed in terms of the Green's function $G_{CL}^<(t, t') = -i \langle u^L(t') u^C(t)^T \rangle^T$. Since operators u and \dot{u} are related in Fourier space as $\dot{u}[\omega] = -i\omega u[\omega]$, we can eliminate the derivative and get,

$$I_L = -\frac{1}{2\pi} \int_{-\infty}^{\infty} \text{Tr} (V^{LC} G_{CL}^<[\omega]) \omega d\omega. \quad (132)$$

Using the result derived earlier relating the mixed lead-center Green's function to the center-only Green's function (transpose of Eq. (124) with G_0 replaced by G) and applying the Langreth theorem, Eq. (99), we have $G_{CL}^<[\omega] = G_{CC}^r[\omega] V^{CL} g_L^<[\omega] + G_{CC}^<[\omega] V^{CL} g_L^a[\omega]$. The expression for the energy current is then given by

$$I_L = -\frac{1}{2\pi} \int_{-\infty}^{+\infty} d\omega \omega \text{Tr} \left(G^r[\omega] \Sigma_L^<[\omega] + G^<[\omega] \Sigma_L^a[\omega] \right), \quad (133)$$

where $\Sigma_L(\tau, \tau') = V^{CL} g_L(\tau, \tau') V^{LC}$. For notational simplicity, we have dropped the subscript C on the Green's functions denoting the central region. We can obtain a symmetrized expression with respect to left and right lead and make it explicitly real,

$$\begin{aligned} I &= \frac{1}{4} (I_L + I_L^* - I_R - I_R^*) = \frac{1}{4\pi} \int_0^{\infty} d\omega \omega \\ &\text{Tr} \left\{ (G^r - G^a) (\Sigma_R^< - \Sigma_L^<) + iG^< (\Gamma_R - \Gamma_L) \right\}, \end{aligned} \quad (134)$$

where $\Gamma_\alpha = i(\Sigma_\alpha^r - \Sigma_\alpha^a)$. Equation (133) or (134) is valid for any finite temperature differences of the leads.

We define the thermal conductance as

$$\sigma = \lim_{\Delta T \rightarrow 0} \frac{I}{\Delta T} = \frac{\delta I}{\delta T}, \quad (135)$$

where ΔT is the difference of the temperatures between the leads, such that $T_L = T + \Delta T/2$ and $T_R = T - \Delta T/2$.

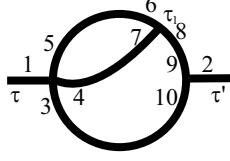


Fig. 7. The 13th Feynman diagram for the nonlinear self-energy Σ_n with labelling.

To take the limit $\Delta T \rightarrow 0$ explicitly, we introduce variational derivatives of the Green's functions, self-energies, or current, in the sense, e.g.,

$$\frac{\delta G}{\delta T} = \lim_{\Delta T \rightarrow 0} \frac{G(T_L, T_R) - G(T, T)}{T_L - T_R}. \quad (136)$$

This is different from varying the temperature of the whole system. The variational derivation measures the response of the system with a fixed overall temperature T and varying only the temperatures of the leads with respect to an average temperature. With the variation derivative defined, we can express the conductance in a form similar to the Landauer formula (5) for the ballistic transport as [13,136],

$$\sigma = \frac{1}{2\pi} \int_0^\infty d\omega \omega \tilde{T}[\omega] \frac{\partial f(\omega)}{\partial T} \quad (137)$$

with an effective transmission coefficient,

$$\begin{aligned} \tilde{T}[\omega] = & \frac{1}{2} \text{Tr} \left\{ G^r(\Gamma_L + \frac{1}{2}\Gamma_n - S) G^a \Gamma_R \right\} + \\ & \frac{1}{2} \text{Tr} \left\{ G^a \Gamma_L G^r(\Gamma_R + \frac{1}{2}\Gamma_n + S) \right\}, \end{aligned} \quad (138)$$

where the nonlinear effect is reflected in the extra terms, $\Gamma_n = i(\Sigma_n^r - \Sigma_n^a)$ and

$$S = \left[f \frac{\delta \Gamma_n}{\delta T} - i \frac{\delta \Sigma_n^<}{\delta T} \right] \left(\frac{\partial f}{\partial T} \right)^{-1}. \quad (139)$$

When $\Gamma_n = S = 0$, we recover the Caroli formula. We note that the effective transmission $\tilde{T}[\omega]$ is temperature dependent, while the ballistic transmission is not.

3.2.6 Perturbative and mean-field self-energies

The nonlinear self-energy, $\Sigma_n(\tau, \tau')$, is the key quantity in solving the heat transport problem in interacting systems. Clearly, it is impossible to evaluate it exactly. Some form of approximation is unavoidable. As the nonlinear interactions are relatively weak for real systems, perturbative treatment can be reliable for temperatures not too high. The approximation can be improved, at least in principle, if more diagrams can be included.

The diagrams shown in Fig. 5 are for the contour-ordered functions. The rules of Feynman diagrams to formula are as follows: label each leg of a vertex with (j_l, τ_l) where l runs over the legs of all the vertices. A vertex is associated with $T_{j_l, j_{l'}, j_{l''}}(\tau_l, \tau_{l'}, \tau_{l''})$ for a three-body interaction, and similarly for a four-body interaction. If leg

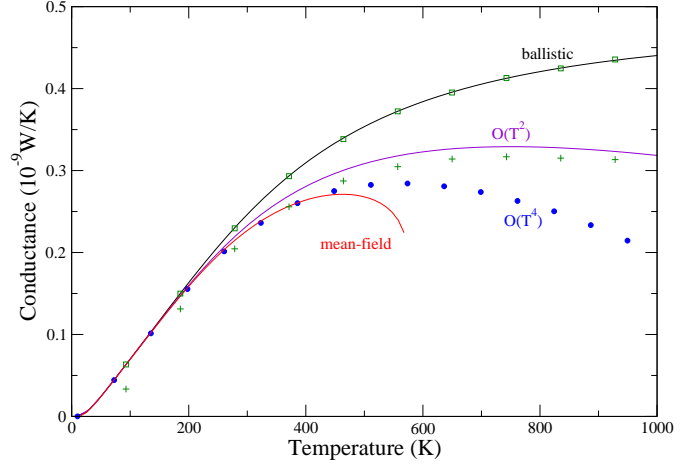


Fig. 8. Thermal conductance as a function of temperature for a 1D junction with three atoms in different approximations. The harmonic spring constants are $k_L = 1.56$, $k_R = 1.44$, $k_C = 1.38$ (eV/(\text{\AA}^2\text{amu})). The coupling between the center and leads is the same as the spring constants of the respective leads. The nonlinear strength is $t = 1.8$ eV/(\text{\AA}^3\text{amu}^{3/2}), with an interaction of the form $(t/3) \sum (u_j - u_{j+1})^3$. Small on-site quadratic potentials are applied to the leads with spring constants $k_L^{\text{onsite}} = 0.006$, and $k_R^{\text{onsite}} = 0.013$ (eV/(\text{\AA}^2\text{amu})). From ref. [12]. The squares and crosses are the molecular dynamics results for the ballistic and nonlinear systems, respectively, from this work. The MD step size is $\Delta t = 3 \times 10^{-16}$ s with 5×10^8 MD steps.

l and l' are connected by a line, associate them with the Green's function $G_{j_l, j_{l'}}^0(\tau_l, \tau_{l'})$. Integrate on the contour all the internal τ variables and sum over the internal site indices j . Since each n -leg vertex has $n - 1$ generalized delta functions in τ , this effectively makes each vertex with one single τ . For example, the 13-th diagram for the self-energy is labelled as shown in Fig. 7, then the associated expression is

$$\sum_{\substack{j_3, j_4, j_5, j_6, \\ j_7, j_8, j_9, j_{10}}} \int d\tau_1 T_{j_1, j_3, j_4, j_5} T_{j_6, j_7, j_8} T_{j_9, j_{10}, j_2} G_{j_3, j_{10}}^0(\tau, \tau') \\ G_{j_5, j_6}^0(\tau, \tau_1) G_{j_4, j_7}^0(\tau, \tau_1) G_{j_8, j_9}^0(\tau_1, \tau'). \quad (140)$$

High order perturbative treatment is computationally too costly except for very small systems. Mean-field approximations are usually used. In such approximations, only certain selected diagrams are used, with the replacement of G^0 by the full Green's function G . So the self-energy is considered a functional of G instead G^0 . For Coulomb-type interactions in electronic transport, GW or even simpler treatments have been used [146,147]. Certain types of self-consistent approximation have the added advantage that the energy conservation [148,145] is fulfilled in the sense $I_L + I_R = 0$. This may not be the case if bare self-energies are used.

In ref. [130], only the first self-energy diagram in Fig. 5 is used. We have made a comparison of the first and second order perturbative approximation, and self-consistent mean-field approximation (with the first two diagrams),

see Fig. 8. Our experience with several models [12,13] seems to suggest that mean-field approximation tends to over estimate the nonlinear effect. Additional problem associated with a self-consistent approximation is that the iterations may not converge. Thus, finding a good approximation is still an open challenge for the phonon interactions at high temperatures.

3.3 Classical molecular dynamics with quantum heat-baths

Molecular dynamics (MD) has been used extensively to study thermal transport based on Green-Kubo formula in equilibrium or for nonequilibrium MD with heat source and sink (heat baths). However, since MD follows a purely classical dynamics, quantum effects are not taken into account. There have been some attempts to partially incorporate quantum feature into an MD by scaling the temperature and the thermal conductivity after the simulations [149,150,151]. Given the actual classical simulation temperature T_{MD} with kinetic energy $Nk_B T_{\text{MD}}/2$, where N is the number of degrees of freedom, a new temperature T can be defined by comparing to a quantum harmonic system with the same kinetic energy,

$$Nk_B T_{\text{MD}} = \sum_k \hbar\omega_k \left(\frac{1}{\exp(\hbar\omega_k/(k_B T)) - 1} + \frac{1}{2} \right), \quad (141)$$

where the summation is over the vibrational modes. The conductivity is also scaled by [150]

$$\kappa = \kappa_{\text{MD}} \frac{dT_{\text{MD}}}{dT}, \quad (142)$$

which is effectively multiplying the classical value by the quantum heat capacity of the corresponding harmonic lattice. Both Eq. (141) and (142) are plausible but lack a more rigorous basis. Another approach is the centroid molecular dynamics proposed by Cao and Voth [152,153]. This appears very sophisticated. The main difficulty here is to obtain the temperature-dependent effective potential for the molecular dynamics.

In ref. [154], we proposed a method based on a generalized Langevin dynamics. The quantum Langevin dynamics is well studied [155,156]. However, its use in thermal transport is only recent [157,82]. The idea is to consider a quantum Langevin equation where the degrees of freedom of the leads are eliminated in favoring that of only the central interacting region. This can be performed exactly if the leads and the couplings between the center and leads are linear. Then the central part is treated as a classical system, while the leads retain quantum-mechanical properties. This amounts to a quasi-classical approximation of the quantum Langevin equation [158,159]. Such a treatment also works for electron transport, and electron-phonon interactions [160].

With the Hamiltonian defined by Eq. (1), the corresponding quasi-classical generalized Langevin equation is

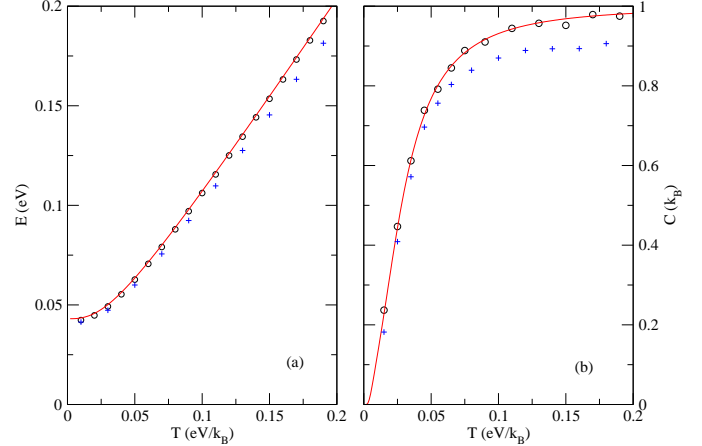


Fig. 9. Energy (a) and heat capacity (b) per degree of freedom for the 1D chain models studied in ref. [154]. The solid lines are exact results for a 1D harmonic chain of length $N = 128$ with periodic boundary condition, while the circles are obtained for the same model from the MD with quantum heat-baths at the ends; the crosses are the MD results of a nonlinear model with an extra quartic onsite potential, $\frac{\mu}{4} \sum u_j^4$, with $\mu = 1 \text{ eV}/(\text{\AA}^4 \text{amu}^2)$.

given by [154]

$$\ddot{u}^C = -K^C u^C + F_n(u^C) - \int_{t_0}^t \Sigma^r(t, t') u^C(t') dt' + \xi_L + \xi_R, \quad (143)$$

where $F_n = -\partial V_n / \partial u^C$ is the nonlinear force, Σ^r is the retarded self-energy of the leads, $\Sigma^r = \Sigma_L^r + \Sigma_R^r$, as used in the NEGF calculation, but in the time domain; $\Sigma_L^r = V^{CL} g_L^r V^{LC}$. A similar equation holds for the right lead Σ_R^r using the right lead surface Green's function.

The noise $\xi_L(t)$ or $\xi_R(t)$ has zero mean and a correlation matrix determined by the temperature and the model of the leads. Using the (surface) density of states, the expression for the correlation can be simplified to get a rather compact result for the spectrum of the noises [82],

$$\tilde{F}[\omega] = \int_{-\infty}^{\infty} \langle \xi_L(t) \xi_L^T(0) \rangle e^{i\omega t} dt = \left(f_L(\omega) + \frac{1}{2} \right) \hbar \Gamma_L[\omega], \quad (144)$$

where $\Gamma_L[\omega] = i(\Sigma_L^r[\omega] - \Sigma_L^a[\omega]) = -2 \text{Im} V^{CL} g_L^r[\omega] V^{LC}$, and $f_L(\omega)$ is the Bose-Einstein distribution function at the temperature of left lead. The situation for the right lead is analogous. The spectrum function $\tilde{F}[\omega]$ is even in ω and is a symmetric, positive semidefinite matrix. A classical limit is obtained if we take $(f_L(\omega) + 1/2)\hbar \approx k_B T_L / \omega$.

The steady state thermal current can be computed in several equivalent ways:

$$\begin{aligned} I_L = -I_R &= -\left\langle \frac{dH_L}{dt} \right\rangle = \langle (\dot{u}^L)^T V^{LC} u^C \rangle \\ &= \langle u^C(t)^T \dot{B}(t) \rangle = \langle \dot{u}^C(t)^T B(t) \rangle, \end{aligned} \quad (145)$$

where $B(t) = -\int_{t_0}^t \Sigma_L^r(t, t') u^C(t') dt' + \xi_L(t)$.

If $V_n = 0$ the linear Langevin equation can be solved analytically. The result for the thermal current reproduces

exactly the Caroli formula [82]. On the other hand, if temperature is sufficiently high (e.g., 1/2 of the Debye temperature), the nonlinear Langevin equation agrees with classical MD result (with appropriate heat baths). For nonlinear systems with $V_n \neq 0$, the equation can be solved numerically. At low temperatures, the transport is mostly ballistic, the dynamics correctly reproduces quantum results and agrees well with NEGF calculation [154]. At the intermediate temperature range, where both quantum and nonlinear effects are strong, the dynamics gives only approximate results. However, we note that the quasi-classical approximation can be systematically improved, if we use the techniques proposed in [161,162,163,164,165,166,167,168]. For example, the leading order correction is obtained if we enlarge the equation set to include variables u^2 , up , and p^2 ($p = \dot{u}$) as independent variables. Thus, the dynamics can provide a nonperturbative solution to the quantum transport problems.

In Fig. 8 we show comparisons of MD and NEGF results. For the ballistic case, the agreement is perfect with very high precision. For the nonlinear system, in order to have a stable MD, we have added an additional quartic potential, $\mu/4 \sum (u_j - u_{j+1})^4$, with $\mu = 0.6 \text{ eV}/(\text{\AA}^4 \text{amu}^2)$ in the simulation, thus the comparison is hardly on an equal footing. The discrepancy at low temperatures between NEGF and the MD has to do with the zero-point motion contribution. In the noise spectrum, Eq. (144), the $1/2$ in $f_L + 1/2$ represents a contribution from zero-point vibration of the quantum oscillators. We can replace $f_L + 1/2$ by $f_L(\omega)$ for $\omega > 0$ and $-f_L(-\omega)$ for $\omega < 0$, and it will not have any effect to the thermal current of a ballistic system. But the removal of the zero-point motions does have some consequences to the nonlinear system under quasi-class approximation.

It is interesting to note that the Langevin dynamics with quantum heat baths also provides a way to compute the equilibrium energy, and by numerical differentiation, the heat capacity of the quantum models. The energy is obtained by the MD averages of the classical expression of kinetic energy plus the potential energy, with a left and right bath at the same temperature. A comparison of the exact and MD results is presented in Fig. 9 for the linear chain. For nonlinear systems in thermal equilibrium, an alternative method is (path-integral) quantum Monte Carlo [169].

3.4 Other treatments of nonlinear effects

In this subsection, we briefly mention several other approaches for treating the nonlinear quantum thermal transport for dielectric materials. In refs. [170,171,172] Michel *et al.* used Hilbert space average method to derive diffusion-like equations on 1D chains, thus justified the Fourier's law and computed the thermal conductivity from Hamiltonian model parameters. These models are idealized so that each site has a band of excited states separated with an energy gap to the ground state. The couplings between the sites are assumed weak. Diffusion equation of

the form, $dP_\mu/dt = \gamma(P_{\mu-1} - 2P_\mu + P_{\mu+1})$, can be derived, where P_μ is the probability that site μ is at excited states. The diffusion constant γ is then related to the thermal conductivity. Segal *et al.* studied thermal rectifying effects of quantum systems with somewhat similar approach of subspace projection, where again diffusion-like rate equations are derived for the occupation of the quantum states [173,174,175], the nonlinearity is introduced by restricting to two-level or finite-level systems. In ref. [176] a master equation approach for more general systems is considered and the Fourier's law of heat conduction is derived. The approximations made always work in diffusive regime. It seems to us that it is difficult to address the issue of transition from ballistic behavior at short time and length scales to diffusive behavior at long time and length scales in the above approaches, but see ref. [177] for such possibilities. In refs. [178,179,180] heat flow through model molecular and nanocrystal junctions is treated using Fermion-golden rule for the rate of phonon relaxations. The Fermi-Pasta-Ulam chain is treated quantum-mechanically in ref. [181]. The authors find an $L^{0.4}$ divergence for the thermal conductivity by considering the relaxation rates of the phonon modes.

4 Electron-phonon interactions

In this section, we extend the NEGF method in subsec. 3.2 to include the electron subsystem and electron-phonon interactions (EPIs). The study of EPI in the context of nanoscale electronic transport is an important field which has attracted intense research recently [6,182]. An extensive discussion of this issue is certainly out of the scope of current review. Here we only concentrate on one special aspect, namely the current induced heating in nanostructures. Different schemes exist in the literature to study this effect [183,184,185,186,187,188,189,190,191,192,193,194]. When the EPI is strong, a canonical transformation is useful to study a minimum model system [133,6,83,193]. But it is not applicable to large systems. On the other hand, perturbative approaches based on the lowest order Born approximation are applicable for relatively weak interactions [184,192,83,194]. Actually, it has already been used in the first principles study [190,191,192]. Hybrid approaches also exist, where the electrons are treated quantum-mechanically, while the phonons use MD with quantum corrections [183,187,188,189]. In our NEGF formalism, we use the mean field method based on the lowest order Born approximation, the so-called self-consistent Born approximation (SCBA).

The Hamiltonian of the whole system is the sum of the electron and phonon part. Consisting with Eq. (1), the electron Hamiltonian reads

$$\mathcal{H}^e = \sum_{\alpha=L,C,R} c_\alpha^\dagger F^\alpha c_\alpha + \sum_{\alpha=L,R} (c_\alpha^\dagger V_e^{\alpha C} c_C + \text{h.c.}) + \sum_{ijk} M_{ij}^k u_k c_i^\dagger c_j, \quad (146)$$

where c_α is a column vector consisting of all the annihilation operators in α region, c_α^\dagger is the corresponding creation operators. $V_e^{\alpha C}$ has similar meaning as $V^{\alpha C}$ in the

phonon Hamiltonian, and $V_e^{\alpha C} = (V_e^{C\alpha})^\dagger$. The last term represents the EPI, where we only keep the first order Taylor expansion about the atomic equilibrium position. M_{ij}^k is the interaction coefficient. We assume that EPI takes place only at the center region, and the subscript C has been omitted.

In ref. [194] we adopt the SCBA to study the coupled electron and phonon transport. All the electron Green's functions are defined as usual [128], e.g.,

$$D^r(t, t') = -i\theta(t - t') \langle [c(t), c^\dagger(t')]_+ \rangle. \quad (147)$$

We use d to denote the free lead Green's function. D_0 and D are the noninteracting and the full electron Green's functions of the center, respectively. The free lead Green's function d can be obtained using the same method as that for phonons ($\alpha = L, R$)

$$d_{\alpha}^{r,a}[\omega] = [(\omega \pm i\eta) - F^\alpha]^{-1}, \quad (148)$$

$$d_{\alpha}^{<}[\omega] = -f_{\alpha}^e[\omega] \left(d_{\alpha}^r[\omega] - d_{\alpha}^a[\omega] \right). \quad (149)$$

$f^e(\omega)$ is the Fermi-Dirac distribution function. The non-interacting electron Green's functions can also be solved exactly

$$D_0^{r,a}[\omega] = [(\omega \pm i\eta) - F^C - \Pi^{r,a}[\omega]]^{-1}, \quad (150)$$

$$D_0^{<,>}[\omega] = D_0^r[\omega] \Pi^{<,>}[\omega] D_0^a[\omega]. \quad (151)$$

The electron self-energy includes contributions from both leads $\Pi = \Pi_L + \Pi_R$, and

$$\Pi_{\alpha}^{r,a,<,>}[\omega] = V_e^{C\alpha} d_{\alpha}^{r,a,<,>}[\omega] V_e^{\alpha C}. \quad (152)$$

The full Green's function D follows the same relations, except that the self-energies include EPI contribution. The notations used in Eq. (147) to (152) for electron Green's functions and self-energies are not standard. As we have already used G and Σ for the phonons in earlier sections, D and Π are used here for the electrons.

The central problem is how to get Π_{epi} and Σ_{epi} . The SCBA includes only the lowest order self-energies. For Π_{epi} , there are two Feynman diagrams, the first two in Fig. 5 with modifications. In the first one, only half of the circle represents phonons, and all other lines represent electrons. In the second one, only the vertical line represents phonons, and all others are electrons. For Σ_{epi} , there is only one diagram, the first one in Fig. 5 with the circle representing electrons. The coefficients also change to i , $-i$, and $-i$, respectively. The rules to translate the diagrams into expressions remain the same as for phonons, provided that the interaction vertex is defined by

$$M_{ij}^k(\tau_i, \tau_j, \tau_k) = M_{ij}^k \delta(\tau_i, \tau_j) \delta(\tau_i, \tau_k). \quad (153)$$

Mean field method is used to calculate the self-energies and the Green's functions.

The electron and the energy current can be expressed via the Green's functions. The electronic current out of the lead α ($\alpha = L, R$) is [76,127,128]

$$J_{\alpha} = e \int_{-\infty}^{+\infty} \frac{d\omega}{2\pi} \text{Tr} \{ D^{>}[\omega] \Pi_{\alpha}^{<}[\omega] - D^{<}[\omega] \Pi_{\alpha}^{>}[\omega] \}. \quad (154)$$

Similarly, the energy current is

$$I_{\alpha}^e = \int_{-\infty}^{+\infty} \frac{d\omega}{2\pi} \omega \text{Tr} \{ D^{>}[\omega] \Pi_{\alpha}^{<}[\omega] - D^{<}[\omega] \Pi_{\alpha}^{>}[\omega] \}. \quad (155)$$

The heat current can be obtained from Eqs. (154–155) as $I_{\alpha}^h = I_{\alpha}^e - \mu_{\alpha} J_{\alpha} / e$. μ_{α} is the chemical potential of the lead α . For phonons the energy and the heat current are the same. In the presence of EPI, there is energy exchange between the electron and the phonon subsystem, which is the source of Joule heating. The use of SCBA guarantees the energy and electronic current conservation [194,147], so that we can write them in symmetric forms. The electronic current is

$$J = e \int_{-\infty}^{+\infty} \frac{d\omega}{2\pi} \tilde{T}^e[\omega] (f_L^e[\omega] - f_R^e[\omega]). \quad (156)$$

The effective transmission coefficient reads (ω omitted)

$$\tilde{T}^e = \text{Tr} \left\{ \frac{1}{2} [D^r(\Lambda_L^e + \frac{1}{2} \Lambda_{\text{epi}} - X_{\text{epi}}) D^a \Lambda_R^e + D^a \Lambda_L^e D^r(\Lambda_R^e + \frac{1}{2} \Lambda_{\text{epi}} + X_{\text{epi}})] \right\}, \quad (157)$$

$$X_{\text{epi}} = \frac{\frac{1}{2}(f_R^e + f_L^e) \Lambda_{\text{epi}} + i \Pi_{\text{epi}}^{<}}{f_L^e - f_R^e}, \quad (158)$$

$\Lambda_{\alpha}^e = i(\Pi_{\alpha}^r - \Pi_{\alpha}^a)$ ($\alpha = L, R$) and $\Lambda_{\text{epi}} = i(\Pi_{\text{epi}}^r - \Pi_{\text{epi}}^a)$. The total energy current includes electron and phonon contributions

$$I^t = \int_{-\infty}^{+\infty} \frac{d\omega}{2\pi} \omega \left\{ \tilde{T}^e[\omega] (f_L^e(\omega) - f_R^e(\omega)) + \frac{1}{2} \tilde{T}^{\text{ph}}[\omega] (f_L(\omega) - f_R(\omega)) \right\}, \quad (159)$$

where \tilde{T}^{ph} is similar to eq. (138), except that Γ_n is replaced by $\Gamma_{\text{epi}} = i(\Sigma_{\text{epi}}^r - \Sigma_{\text{epi}}^a)$, and S by

$$S_{\text{epi}} = \frac{\frac{1}{2}(f_R + f_L) \Gamma_{\text{epi}} - i \Sigma_{\text{epi}}^{<}}{f_L - f_R}. \quad (160)$$

Here we have corrected a sign error in Eq. (22) of ref. [194]. Heat generation during the current flow can also be written in terms of Green's functions [194],

$$Q = i \int_{-\infty}^{+\infty} \frac{d\omega'}{2\pi} \int_{-\infty}^{+\infty} \frac{d\omega}{2\pi} \omega \sum_{nmikl} D_{nm}^{>}[\omega'] M_{mi}^k G_{kl}^{<}[\omega] D_{ij}^{<}[\omega' - \omega] M_{jn}^l. \quad (161)$$

Equation (161) can be used to study the Joule heating in nonequilibrium molecular junctions. Similar results have also been derived by other authors [83,192,193].

In Fig. 10, we show the heat generation as a function of onsite energy of a single quantum dot coupled with two 1D leads, calculated using Eq. (161). When the applied bias is less than the phonon energy ω , there is no heating. When the bias energy is slightly larger than ω and less than 2ω , there are two energies where the heat generation

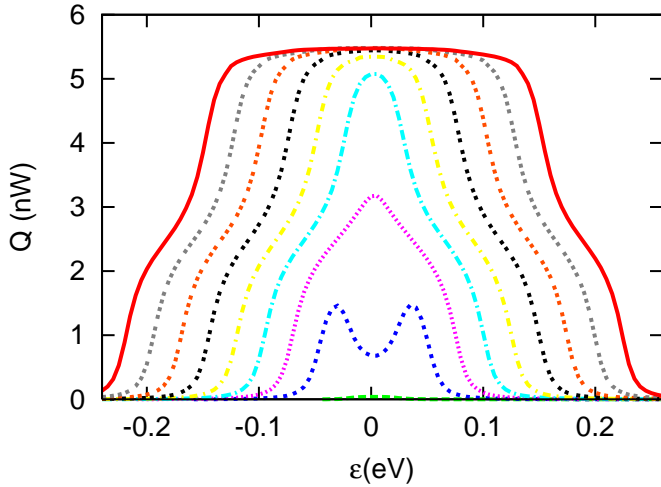


Fig. 10. Heat generation Q as a function of electrical onsite energy ε for a quantum dot coupled with 1D leads (ref. [194]). From the inner to the outer side, the applied biases are $V = 0.05$ to 0.50 V with an increment of 0.05 V, respectively.

is the largest. These two peak positions are approximately at $-0.5 \text{ eV} + \omega$ and $0.5 \text{ eV} - \omega$. They merge into a single one at a bias of 2ω until it reaches saturation. After that, this peak broadens to a ladder. These interesting features are unique properties of nanostructures, absent in the bulk case.

5 Experiments in nanostructure heat transport

Some of the earliest direct mesoscopic thermal conductance measurements are done on patterned semiconductor structures with cross section sizes of few hundred nanometers [195]. The calorimetry on such a small scale is a challenge, but very promising, e.g., one may count the number of phonons in a nanostructure [196]. In 2000, such type of devices is used to confirm the universal thermal conductance quanta at temperatures below 1 K [26]. Bridges of catenoidal shape are used, based on an earlier theoretical analysis that such geometric shape gives the maximum transmission [17]. Other extensively studied systems are carbon nanotubes. Initially, only mats or rope bundle or film form can be measured, given a relatively low thermal conductivity of order $100 \text{ W}/(\text{mK})$ at room temperature [197,198,199]. The initial theoretical predictions by molecular dynamics for single nanotubes along the axial direction are much higher [200,201]. Indeed, individual multiwalled and single wall carbon nanotube measurements became possible, and the measured values are about $3000 \text{ W}/(\text{mK})$ at room temperature by several groups [202,203,204,205]. Typically, these measurements use tube lengths of few μm . The length dependence effects are analyzed in [205] and observed in [206]. In ref. [207], it is claimed that ballistic phonon transport is consistent with experimental data, even for temperatures as high as 900 K for submicron tube lengths. Another class of systems is

individual silicon nanowires [208,209,210]. It has been observed that rough and small diameter silicon nanowires have a low thermal conductivity; this property can be used for good thermoelectric applications [210]. Thermal rectification effect has been observed in carbon nanotubes with one side of the tube deposited with $\text{C}_9\text{H}_{16}\text{Pt}$ [211]. However, the observed effect is rather small, at a level of few percents. Another way of explicit control of the heat flow in nanostructure is using a tunable thermal links [212], where a multiwalled carbon nanotube is cut and the outer layers of the tube can be moved mechanically with respect to the inner layers. Much large modulation is then possible. In ref. [213], it is demonstrated that the carbon nanotube heat conduction is rather robust against bending and deformation. Phonon transport in point contact of metal-insulator is studied in ref. [214]. The studies of thermal transport at an individual molecular level are scarce. But impressive progress is made recently [215,216,217]. In ref. [217], alkane chain anchored to a gold substrate is heated to about 1100 K, the propagation of the heat waves is timed. This timing information indicates that the heat transport at such scale of few nanometers is ballistic. The thermal conductance was inferred to be $0.05 \text{ nW}/\text{K}$.

6 Conclusion

Using a general junction model as an illustration, we consider the problem of theoretical modeling of heat transport in nanojunctions. If the nonlinear forces can be omitted, this would be the case if temperature is low or the sizes of the system is small, the Landauer formula gives a very good description of the ballistic thermal transport. We give a derivation of the Landauer formula from the wave scattering point of view. A derivation from NEGF is also outlined as a special case of the more general nonlinear result. Several different ways of calculating the transmission coefficient appearing in the Landauer formula are reviewed. Among the alternative computational methods, the calculation based on Caroli formula and the iterative algorithm of the surface Green's functions is the most efficient computationally for the total transmission coefficient $T[\omega]$. The mode-matching method gives the results of transmission of each mode to every other mode, thus containing more information. The relation of the two approaches is clarified. The transfer matrix method and Picard formula are theoretically interesting, but they may not be practical in actual calculations, e.g., the transfer matrix can be numerically unstable for large systems. In summary, for the ballistic transport, efficient computational algorithms exist for arbitrary complex systems with numbers of atoms less than about 10^3 .

For the treatment of nonlinear effects, it is still a great challenge. We first presented a phenomenological treatment of the nonlinear effect using the information on the mean free path. A systematic development of the nonequilibrium Green's function method is given. We emphasize the use of contour ordered Green's functions and the equations of motion defined on the Keldysh contour. To do this, we must generalize the θ and δ functions, and also

generalize the Heisenberg equation to the contour. Quantum field-theoretic method is used to develop the Dyson equations relating the ballistic system and interacting system. The nonlinear effect can be taken into account if the nonlinear self energy Σ_n can be obtained accurately. Perturbative expansion and mean-field approximation to the nonlinear self-energy are possible. The Landauer formula can be generalized formally in the nonlinear case, except now the transmission function is temperature dependent. For small systems at not too high temperatures (e.g., $T < 400$ K), the results with these approximations are reliable. But for large systems or higher temperatures, the approximation can break down. A more promising method to handle large systems and high temperatures is molecular dynamics. With the quantum heat baths discussed in this review, the quantum effect can be partially taken into account and it is even possible to correct the quasi-classical approximation.

We also reviewed briefly methods for electron-phonon interactions. This is an important area where many interesting effects can be investigated experimentally, and it is also very relevant to the electronic industry. NEGF and other methods will play important role in the study. We also give a quick review of the experimental status of thermal transport problems in nanostructures. To a theoretical or computational modelling scientist, it is easy to work with small systems, while it is hard to an experimentalist to manipulate and measure heat at the molecular level. We hope that the two sides of approaches will converge well in the near future.

For the convenience of reader, we have put up a webpage [218] to post some of the implementations of algorithms, which may clarify the doubts and subtleties in understanding them.

Acknowledgments

Parts of the results under review were in collaboration with Nan Zeng and Chee-Kwan Gan. The authors thanks for discussions with Baowen Li, Jiangbin Gong, Pawel Keblinski, Saikong Chin, Yong Xu, and Jinhua Lan. This work is supported in part by a faculty research grant R-144-000-173-112/101 of NUS.

References

1. R.E. Peierls, *Quantum Theory of Solids* (Oxford Univ., 1955)
2. P. Carruthers, *Rev. Mod. Phys.* **33**, 92 (1961)
3. H. Spohn, *J. Stat. Phys.* **124**, 1041 (2006)
4. D.G. Cahill, W.K. Ford, K.E. Goodson, G.D. Mahan, A. Majumdar, H.J. Maris, R. Merlin, S.R. Phillpot, *J. Appl. Phys.* **93**, 793 (2003)
5. G. Chen, D. Borca-Tasciuc, R.G. Yang, in *Encyclopedia of Nanoscience and Nanotechnology*, edited by H.S. Nalwa (Amer. Sci. Publ., 2004), Vol. 7, p. 429
6. M. Galperin, M.A. Ratner, A. Nitzan, *J. Phys.:Condens. Matter* **19**, 103201 (2007)
7. P.F. Meier, *Phys. kondens. Materie* **8**, 241 (1969)
8. G.D. Mahan, *Phys. Rep.* **145**, 251 (1987)
9. S. Lepri, R. Livi, A. Politi, *Phys. Rep.* **377**, 1 (2003)
10. A.J.H. McGaughey, M. Kaviani, *Adv. in Heat Transf.* **39**, 169 (2006)
11. P. Heino, *J. Comput. Theor. Nanoscience* **4**, 896 (2007)
12. J.S. Wang, J. Wang, N. Zeng, *Phys. Rev. B* **74**, 033408 (2006)
13. J.S. Wang, N. Zeng, J. Wang, C.K. Gan, *Phys. Rev. E* **75**, 061128 (2007)
14. R. Landauer, *IBM J. Res. Dev.* **1**, 223 (1957)
15. R. Landauer, *Philos. Mag.* **21**, 863 (1970)
16. D.E. Angelescu, M.C. Cross, M.L. Roukes, *Superlattices Microstruc.* **23**, 673 (1998)
17. L.G.C. Rego, G. Kirczenow, *Phys. Rev. Lett.* **81**, 232 (1998)
18. L.G.C. Rego, *Phys. Stat. Sol. (a)* **187**, 239 (2001)
19. M.P. Blencowe, *Phys. Rev. B* **59**, 4992 (1999)
20. M. Blencowe, *Phys. Rep.* **395**, 159 (2004)
21. N. Mingo, D.A. Broido, *Phys. Rev. Lett.* **95**, 096105 (2005)
22. M.J. Frisch, et al., gaussian 03, Revision C.02 (Gaussian Inc., Wallingford, 2004)
23. J. Wang, J.S. Wang, cond-mat/0509092
24. J.B. Pendry, *J. Phys. A: Math. Gen.* **16**, 2161 (1983)
25. M.P. Blencowe, V. Vitelli, *Phys. Rev. A* **62**, 052104 (2000)
26. K. Schwab, E.A. Henriksen, J.M. Worlock, M.L. Roukes, *Nature* **404**, 974 (2000)
27. O. Chiatti, J.T. Nicholls, Y.Y. Proskuryakov, N. Lumpkin, I. Farrer, D.A. Ritchie, *Phys. Rev. Lett.* **97**, 056601 (2006)
28. M. Meschke, W. Guichard, J.P. Pekola, *Nature* **444**, 187 (2006)
29. D.H. Santamore, M.C. Cross, *Phys. Rev. B* **63**, 184306 (2001)
30. D.H. Santamore, M.C. Cross, *Phys. Rev. Lett.* **87**, 115502 (2001)
31. M.C. Cross, R. Lifshitz, *Phys. Rev. B* **64**, 085324 (2001)
32. C.M. Chang, M.R. Geller, *Phys. Rev. B* **71**, 125304 (2005)
33. S.X. Qu, M.R. Geller, *Phys. Rev. B* **70**, 085414 (2004)
34. A.N. Cleland, D.R. Schmidt, C.S. Yung, *Phys. Rev. B* **64**, 172301 (2001)
35. Y. Tanaka, F. Yoshida, S. Tamura, *Phys. Stat. Sol. (c)* **1**, 2625 (2004)
36. Y. Tanaka, F. Yoshida, S. Tamura, *Phys. Rev. B* **71**, 205308 (2005)
37. W.X. Li, K.Q. Chen, W. Duan, J. Wu, B.L. Gu, *J. Phys. D: Appl. Phys.* **36**, 3027 (2003)
38. W.X. Li, K.Q. Chen, W. Duan, J. Wu, B.L. Gu, *J. Phys.: Condens. Matter* **16**, 5049 (2004)
39. W.X. Li, K.Q. Chen, W. Duan, J. Wu, B.L. Gu, *Appl. Phys. Lett.* **85**, 822 (2004)
40. K.Q. Chen, W.X. Li, W. Duan, Z. Shuai, B.L. Gu, *Phys. Rev. B* **72**, 045422 (2005)
41. W.Q. Huang, K.Q. Chen, Z. Shuai, L. Wang, W. Hu, B.S. Zou, *J. Appl. Phys.* **98**, 093524 (2005)
42. W. Li, K. Chen, *Phys. Lett. A* **357**, 378 (2006)
43. L.M. Tang, L.L. Wang, K.Q. Chen, W.Q. Huang, B.S. Zou, *Appl. Phys. Lett.* **88**, 163505 (2006)
44. W.X. Li, T. Liu, C. Liu, *Appl. Phys. Lett.* **89**, 163104 (2006)
45. Y. Ming, Z.X. Wang, Z.J. Ding, *Phys. Lett. A* **350**, 302 (2006)

46. X.F. Peng, K.Q. Chen, B.S. Zou, Y. Zhang, *Appl. Phys. Lett.* **90**, 193502 (2007)
47. P. Yang, Q. feng Sun, H. Guo, B. Hu, *Phys. Rev. B* **75**, 235319 (2007)
48. J.D. Lu, L. Shao, Y.L. Hou, L. Yi, *Chin. Phys. Lett.* **24**, 793 (2007)
49. Y. Wang, L.L. Wang, L.M. Tang, B.S. Zou, L.H. Zhao, *J. Phys. D: Appl. Phys.* **40**, 7159 (2007)
50. R. Prasher, T. Tong, A. Majumdar, *J. Appl. Phys.* **102**, 104312 (2007)
51. P. Yang, Ph.D. thesis, McGill Univ. (2004)
52. J. Wang, J.S. Wang, *Phys. Rev. B* **74**, 054303 (2006)
53. N.W. Ashcroft, N.D. Mermin, *Solid State Physics* (Saunders College, 1976)
54. R.J. Hardy, *Phys. Rev.* **132**, 168 (1963)
55. P.A. Khomyakov, G. Brocks, *Phys. Rev. B* **70**, 195402 (2004)
56. H. Zhao, J.B. Freund, *J. Appl. Phys.* **97**, 024903 (2005)
57. K. Cho, J. Ushida, M. Bamba, *J. Phys. Soc. Jpn.* **74**, 3088 (2005)
58. J. Velez, W. Butler, *J. Phys.: Condens. Matter* **16**, R637 (2004)
59. T. Ando, *Phys. Rev. B* **44**, 8017 (1991)
60. P.A. Khomyakov, G. Brocks, V. Karpan, M. Zwierzycki, P.J. Kelly, *Phys. Rev. B* **72**, 035450 (2005)
61. W.H. Press, S.A. Teukolsky, W.T. Vetterling, B.P. Flannery, *Numerical Recipes: The Art of Scientific Computing*, 3rd edn. (Cambridge Univ., 2007)
62. D.Y. Ting, E.T. Yu, T.C. McGill, *Phys. Rev. B* **45**, 3583 (1992)
63. D.Y. Ting, *Microelec. J.* **30**, 985 (1999)
64. P. Tong, B. Li, B. Hu, *Phys. Rev. B* **59**, 8639 (1999)
65. E. Maciá, *Phys. Rev. B* **61**, 6645 (2000)
66. V.B. Antonyuk, M. Larsson, A.G. Mal'shukov, K.A. Chao, *Semicond. Sci. Technol.* **20**, 347 (2005)
67. L.S. Cao, R.W. Peng, R.L. Zhang, X.F. Zhang, M. Wang, X.Q. Huang, A. Hu, S.S. Jiang, *Phys. Rev. B* **72**, 214301 (2005)
68. Y.M. Zhang, S.J. Xiong, *Phys. Rev. B* **72**, 115305 (2005)
69. Y.M. Zhang, C.H. Xu, S.J. Xiong, *Chin. Phys. Lett.* **24**, 1017 (2007)
70. P.G. Murphy, J.E. Moore, *Phys. Rev. B* **76**, 155313 (2007)
71. H. Yin, R. Tao, arXiv:0709.3681
72. J.L. Pichard, Ph.D. thesis, Univ. of Paris at Orsay (1984)
73. C.W.J. Beenakker, *Rev. Mod. Phys.* **69**, 731 (1997)
74. L.C. Botten, A.A. Asatryan, N.A. Nicorovici, R.C. McPhedran, C.M. de Sterke, *Physica B* **394**, 320 (2007)
75. C. Caroli, R. Combescot, P. Nozieres, D. Saint-James, *J. Phys. C: Solid St. Phys.* **4**, 916 (1971)
76. Y. Meir, N.S. Wingreen, *Phys. Rev. Lett.* **68**, 2512 (1992)
77. A. Ozpineci, S. Ciraci, *Phys. Rev. B* **63**, 125415 (2001)
78. D. Segal, A. Nitzan, P. Hänggi, *J. Chem. Phys.* **119**, 6840 (2003)
79. N. Mingo, L. Yang, *Phys. Rev. B* **68**, 245406 (2003)
80. W. Zhang, T.S. Fisher, N. Mingo, *Numer. Heat Transf. Part B* **51**, 333 (2007)
81. T. Yamamoto, K. Watanabe, *Phys. Rev. Lett.* **96**, 255503 (2006)
82. A. Dhar, D. Roy, *J. Stat. Phys.* **125**, 805 (2006)
83. M. Galperin, A. Nitzan, M.A. Ratner, *Phys. Rev. B* **75**, 155312 (2007)
84. M. Paulsson, cond-mat/0210519
85. D.H. Lee, J.D. Joannopoulos, *Phys. Rev. B* **23**, 4997 (1981)
86. F. Guinea, C. Tejedor, F. Flores, E. Louis, *Phys. Rev. B* **28**, 4397 (1983)
87. M.P.L. Sancho, J.M.L. Sancho, J. Rubio, *J. Phys. F: Met. Phys.* **14**, 1205 (1984)
88. M.P.L. Sancho, J.M.L. Sancho, J. Rubio, *J. Phys. F: Met. Phys.* **15**, 851 (1985)
89. A. Umerski, *Phys. Rev. B* **55**, 5266 (1997)
90. S. Sanvito, C.J. Lambert, J.H. Jefferson, A.M. Bratkovsky, *Phys. Rev. B* **59**, 11936 (1999)
91. P.S. Krstić, X.G. Zhang, W.H. Butler, *Phys. Rev. B* **66**, 205319 (2002)
92. D.S. Fisher, P.A. Lee, *Phys. Rev. B* **23**, 6851 (1981)
93. D.W. Brenner, O.A. Shenderova, J.A. Harrison, S.J. Stuart, B. Ni, S.B. Sinnott, *J. Phys.: Condens. Matter* **14**, 783 (2002)
94. N. Kondo, T. Yamamoto, K. Watanabe, *Jpn. J. Appl. Phys.* **45**, L963 (2006)
95. T. Yamamoto, Y. Nakazawa, K. Watanabe, *New J. Phys.* **9**, 245 (2007)
96. P.K. Schelling, S.R. Phillpot, P. Keblinski, *Appl. Phys. Lett.* **80**, 2484 (2002)
97. B. Becker, P.K. Schelling, S.R. Phillpot, *Phys. Stat. Sol. (c)* **1**, 2955 (2004)
98. P.K. Schelling, S.R. Phillpot, P. Keblinsk, *J. Appl. Phys.* **95**, 6082 (2004)
99. A. Bodapati, P.K. Schelling, P. Keblinski, preprint
100. T. Yamamoto, S. Watanabe, K. Watanabe, *Phys. Rev. Lett.* **92**, 075502 (2004)
101. T. Yamamoto, K. Watanabe, K. Mii, *Phys. Rev. B* **70**, 245402 (2004)
102. K. Saito, J. Nakamura, A. Natori, *Phys. Rev. B* **76**, 115409 (2007)
103. J. Wang, J.S. Wang, *Appl. Phys. Lett.* **90**, 241908 (2007)
104. J. Wang, J.S. Wang, *J. Phys.:Condens. Matter* **19**, 236211 (2007)
105. W. Zhang, T.S. Fisher, N. Mingo, *J. Heat Transf.* **129**, 483 (2007)
106. W. Zhang, N. Mingo, T.S. Fisher, *Phys. Rev. B* **76**, 195429 (2007)
107. M. Morooka, T. Yamamoto, K. Watanabe, *Phys. Rev. B* **77**, 033412 (2008)
108. N. Mingo, D.A. Stewart, D.A. Broido, D. Srivastava, *Phys. Rev. B* **77**, 033418 (2008)
109. K.R. Patton, M.R. Geller, *Phys. Rev. B* **64**, 155320 (2001)
110. J. Wang, J.S. Wang, *Appl. Phys. Lett.* **88**, 111909 (2006)
111. S. Datta, *Electronic Transport in Mesoscopic Systems* (Cambridge Univ. Press, 1995)
112. Q. Zheng, G. Su, J. Wang, H. Guo, *Eur. Phys. J. B* **25**, 233 (2002)
113. J. Callaway, *Phys. Rev.* **113**, 1046 (1959)
114. M. Roufousse, P.G. Klemens, *Phys. Rev. B* **7**, 5379 (1973)
115. D.J. Ecsedy, P.G. Klemens, *Phys. Rev. B* **15**, 5957 (1977)
116. Y. Xiao, X.H. Yan, J.X. Cao, J.W. Ding, *J. Phys. Condens. Matter* **15**, L341 (2003)
117. J.X. Cao, X.H. Yan, Y. Xiao, J.W. Ding, *Phys. Rev. B* **69**, 073407 (2004)
118. S.P. Hepplestone, G.P. Srivastava, *Phys. Rev. B* **74**, 165420 (2006)
119. S.P. Hepplestone, G.P. Srivastava, *J. Phys.: conf. ser.* **61**, 414 (2007)

120. Y. Gu, Y. Chen, Phys. Rev. B **76**, 134110 (2007)
121. J. Schwinger, J. Math. Phys. (New York) **2**, 407 (1961)
122. L.P. Kadanoff, G. Baym, *Quantum Statistical Mechanics* (Benjamin/Cummings, 1962)
123. L.V. Keldysh, Soviet Phys. JETP **20**, 1018 (1965)
124. M. Bonitz, ed., *Progress in Nonequilibrium Green's Functions* (World Scientific, 2000)
125. M. Bonitz, D. Semkat, eds., *Progress in Nonequilibrium Green's Functions II* (World Scientific, 2003)
126. M. Wagner, Phys. Rev. B **44**, 6104 (1991)
127. A.P. Jauho, N.S. Wingreen, Y. Meir, Phys. Rev. B **50**, 5528 (1994)
128. H. Haug, A.P. Jauho, *Quantum Kinetics in Transport and Optics of Semiconductors* (Springer, 1996)
129. S. Ciraci, A. Buldum, I.P. Batra, J. Phys.:Condens. Matter **13**, R537 (2001)
130. N. Mingo, Phys. Rev. B **74**, 125402 (2006)
131. H.P. Liu, L. Yi, Chin. Phys. Lett. **23**, 3194 (2006)
132. S. Doniach, E.H. Sondheimer, *Green's Functions for Solid State Physicists* (W. A. Benjamin, 1974)
133. G.D. Mahan, *Many-Particle Physics*, 3rd edn. (Kluwer Academic, 2000)
134. H. Bruus, K. Flensberg, *Many-Body Quantum Theory in Condensed Matter Physics, an introduction* (Oxford Univ. Press, 2004)
135. D.C. Langreth, in *Linear and Nonlinear Electron Transport in Solids*, edited by J.T. Devreese, E. van Doren (Plenum, 1976), pp. 3–32
136. N. Zeng, Ph.D. thesis, National Univ. Singapore (2007)
137. A.A. Abrikosov, L.P. Gorkov, I.E. Dzyaloshinski, *Methods of Quantum Field Theory in Statistical Physics* (Dover Publ., 1963)
138. A.L. Fetter, J.D. Walecka, *Quantum Theory of Many-Particle Systems* (McGraw-Hill, 1971)
139. A.M. Zagoskin, *Quantum Theory of Many-Body Systems* (Springer, 1998)
140. D.J. Amit, *Field Theory, the Renormalization Group, and Critical Phenomena*, 2nd edn. (World Scientific, 1984)
141. P. Procacci, G. Cardini, R. Righini, S. Califano, Phys. Rev. B **45**, 2113 (1992)
142. R.G.D. Valle, P. Procacci, Phys. Rev. B **46**, 6141 (1992)
143. R.G.D. Valle, P. Procacci, J. Comput. Phys. **165**, 428 (2000)
144. C. Niu, D.L. Lin, T.H. Lin, J. Phys.:Condens. Matter **11**, 1511 (1999)
145. R. van Leeuwen, N.E. Dahlen, G. Stefanucci, C.O. Almbladh, U. von Barth, in *Time-Dependent Density Functional Theory*, edited by M.A.L. Marques, et al. (Springer, 2006), chap. 3
146. K.S. Thygesen, A. Rubio, J. Chem. Phys. **126**, 091101 (2007)
147. K.S. Thygesen, A. Rubio, arXiv:0710.0482
148. G. Baym, Phys. Rev. **127**, 1391 (1962)
149. C.Z. Wang, C.T. Chan, K.M. Ho, Phys. Rev. B **42**, 11276 (1990)
150. Y.H. Lee, R. Biswas, C.M. Soukoulis, C.Z. Wang, C.T. Chan, K.M. Ho, Phys. Rev. B **43**, 6573 (1991)
151. J. Li, L. Porter, S. Yip, J. Nucl. Mat. **255**, 139 (1998)
152. J. Cao, G.A. Voth, J. Chem. Phys. **99**, 10070 (1993)
153. Y. Yonetani, K. Kinugawa, J. Chem. Phys. **120**, 10624 (2004)
154. J.S. Wang, Phys. Rev. Lett. **99**, 160601 (2007)
155. K. Lindenberg, B.J. West, *The Nonequilibrium Statistical Mechanics of Open and Closed Systems* (VCH, 1990)
156. P. Hänggi, G.L. Ingold, Chaos **15**, 026105 (2005)
157. A. Dhar, D. Sen, Phys. Rev. B **73**, 085119 (2006)
158. A. Schmid, J. Low Temp. Phys. **49**, 609 (1982)
159. U. Weiss, *Quantum Dissipative Systems*, 2nd edn. (World Scientific, 1999)
160. J.T. Lü, J.S. Wang, arXiv:08xx.xxxx
161. L.E. Ballentine, S.M. McRae, Phys. Rev. A **58**, 1799 (1998)
162. O.V. Prezhdo, Y.V. Pereverzev, J. Chem. Phys. **113**, 6557 (2000)
163. E. Pahl, O.V. Prezhdo, J. Chem. Phys. **116**, 8704 (2002)
164. E.M. Heatwole, O.V. Prezhdo, J. Chem. Phys. **122**, 234109 (2005)
165. O.V. Prezhdo, Theor. Chem. Acc. **116**, 206 (2006)
166. D. Barik, B.C. Bag, D.S. Ray, J. Chem. Phys. **119**, 12973 (2003)
167. D. Barik, D.S. Ray, J. Chem. Phys. **121**, 1681 (2004)
168. A.P. Horsfield, D.R. Bowler, A.J. Fisher, T.N. Todorov, C.G. Sánchez, J. Phys.:Condens. Matter **16**, 8251 (2004)
169. D.P. Landau, K. Binder, *A Guide to Monte Carlo Simulations in Statistical Physics*, 2nd edn. (Cambridge Univ. Press, 2005)
170. M. Michel, G. Mahler, J. Gemmer, Phys. Rev. Lett. **95**, 180602 (2005)
171. M. Michel, J. Gemmer, G. Mahler, Phys. Rev. E **73**, 016101 (2006)
172. M. Michel, J. Gemmer, G. Mahler, Int. J. Mod. Phys. B **20**, 4855 (2006)
173. D. Segal, A. Nitzan, Phys. Rev. Lett. **94**, 034301 (2005)
174. D. Segal, A. Nitzan, J. Chem. Phys. **122**, 194704 (2005)
175. D. Segal, Phys. Rev. B **73**, 205415 (2006)
176. L.A. Wu, D. Segal, arXiv:0711.4599
177. R. Steinigeweg, H.P. Breuer, J. Gemmer, Phys. Rev. Lett. **99**, 150601 (2007)
178. A. Buldum, D.M. Leitner, S. Ciraci, Europhys. Lett. **47**, 208 (1999)
179. D.M. Leitner, P.G. Wolynes, Phys. Rev. E **61**, 2902 (2000)
180. D.M. Leitner, Phys. Rev. B **64**, 094201 (2001)
181. G. Santhosh, D. Kumar, Phys. Rev. E **76**, 021105 (2007)
182. A. Mitra, I. Aleiner, A.J. Millis, Phys. Rev. B **69**, 245302 (2004)
183. A.P. Horsfield, D.R. Bowler, A.J. Fisher, T.N. Todorov, M.J. Montgomery, J. Phys.: Condens. Matter **16**, 3609 (2004)
184. T.N. Todorov, Phil. Mag. B **77**, 965 (1998)
185. N. Agrait, C. Untiedt, G. Rubio-Bollinger, S. Vieira, Phys. Rev. Lett. **88**, 216803 (2002)
186. D. Segal, A. Nitzan, J. Chem. Phys. **117**, 3915 (2002)
187. M.J. Montgomery, T.N. Todorov, A.P. Sutton, J. Phys.: Condens. Matter **14**, 5377 (2002)
188. A.P. Horsfield, D.R. Bowler, A.J. Fisher, T.N. Todorov, C.G. Sánchez, J. Phys.: Condens. Matter **17**, 4793 (2005)
189. A.P. Horsfield, D.R. Bowler, H. Ness, C.G. Sánchez, T.N. Todorov, A.J. Fisher, Rep. Prog. Phys. **69**, 1195 (2006)
190. Y.C. Chen, M. Zwolak, M.D. Ventra, Nano Letters **3**, 1691 (2003)
191. T. Frederiksen, M. Brandbyge, N. Lorente, A.P. Jauho, Phys. Rev. Lett. **93**, 256601 (2004)
192. A. Pecchia, G. Romano, A.D. Carlo, Phys. Rev. B **75**, 035401 (2007)

193. Q.F. Sun, X.C. Xie, Phys. Rev. B **75**, 155306 (2007)
194. J.T. Lü, J.S. Wang, Phys. Rev. B **76**, 165418 (2007)
195. T.S. Tighe, J.M. Worlock, M.L. Roukes, Appl. Phys. Lett. **70**, 2687 (1997)
196. M.L. Roukes, Physica B **263**, 1 (1999)
197. J. Hone, M. Whitney, C. Piskoti, A. Zettl, Phys. Rev. B **59**, R2514 (1999)
198. D.J. Yang, Q. Zhang, G. Chen, S.F. Yoon, J. Ahn, S.G. Wang, Q. Zhou, Q. Wang, J.Q. Li, Phys. Rev. B **66**, 165440 (2002)
199. H. Xie, A. Cai, X. Wang, Phys. Lett. A **369**, 120 (2007)
200. S. Berber, Y.K. Kwon, D. Tománek, Phys. Rev. Lett. **84**, 4613 (2000)
201. J.R. Lukes, H. Zhong, J. Heat Transf. **129**, 705 (2007)
202. P. Kim, L. Shi, A. Majumdar, P.L. McEuen, Phys. Rev. Lett. **87**, 215502 (2001)
203. P. Kim, L. Shi, A. Majumdar, P.L. McEuen, Physica B **323**, 67 (2002)
204. C. Yu, L. Shi, Z. Yao, D. Li, A. Majumdar, Nano Lett. **5**, 1842 (2005)
205. E. Pop, D. Mann, Q. Wang, K. Goodson, H. Dai, Nano Lett. **6**, 96 (2006)
206. Z.L. Wang, D.W. Tang, X.B. Li, X.H. Zheng, W.G. Zhang, L.X. Zheng, Y.T. Zhu, A.Z. Jin, H.F. Yang, C.Z. Gu, Appl. Phys. Lett. **91**, 123119 (2007)
207. H.Y. Chiu, V.V. Deshpande, H.W.C. Postma, C.N. Lau, C. Mikó, L. Forró, M. Bockrath, Phys. Rev. Lett. **95**, 226101 (2005)
208. D. Li, Y. Wu, P. Kim, L. Shi, P. Yang, A. Majumdar, Appl. Phys. Lett. **83**, 2934 (2003)
209. O. Bourgeois, T. Fournier, J. Chaussy, J. Appl. Phys. **101**, 016104 (2007)
210. A.I. Hochbaum, R. Chen, R.D. Delgado, W. Liang, E.C. Garnett, M. Najarian, A. Majumdar, P. Yang, Nature **451**, 163 (2008)
211. C.W. Chang, D. Okawa, A. Majumdar, A. Zettl, Science **314**, 1121 (2006)
212. C.W. Chang, D. Okawa, H. Garcia, T.D. Yuzvinsky, A. Majumdar, A. Zettl, Appl. Phys. Lett. **90**, 193114 (2007)
213. C.W. Chang, D. Okawa, H. Garcia, A. Majumdar, A. Zettl, Phys. Rev. Lett. **99**, 045901 (2007)
214. A. Feher, S.A. Egupov, A.G. Shkorbatov, Low Temp. Phys. **33**, 861 (2007)
215. Z. Ge, D.G. Cahill, P.V. Braun, Phys. Rev. Lett. **96**, 186101 (2006)
216. A. Nitzan, Science **317**, 759 (2007)
217. Z. Wang, J.A. Carter, A. Lagutchev, Y.K. Koh, N.H. Seong, D.G. Cahill, D.D. Dlott, Science **317**, 787 (2007)
218. [Http://staff.science.nus.edu.sg/~phywjs/NEGF/negf.html](http://staff.science.nus.edu.sg/~phywjs/NEGF/negf.html)

